UNIVERSITA' DEGLI STUDI DI PADOVA

Dipartimento di Ingegneria Industriale DII

Corso di Laurea Magistrale in Ingegneria dei Materiali

HYBRIDIZATION OF ADDITIVE MANUFACTURING PROCESSES FOR FABRICATION OF FUNCTIONAL CERAMICS WITH EMBEDDED MICROCHANNELS

Relatore: Dott.sa Giorgia Franchin

Correlatore: Prof. Paolo Colombo

Laureando:

Saverio Valentino 1148564

Anno Accademico 2018/2019

Abstract

This thesis presents the results of a work concerning a novel technology based on the combination of two different additive manufacturing techniques applied to ceramics materials aimed to obtain functional ceramics with embedded microchannel.

Generally, ceramic parts with built-in microchannels are made by first opening the microchannels and then covering them with additional ceramics using the joining method. Methods such as mold embossing and laser machining are generally used for the manufacture of the openings. Nowadays, the most advanced method of manufacturing microchannels within ceramics is the Low temperature co-fired ceramic technology. Nevertheless, these processes are complex, sometimes limited and especially expensive for the production foundry.

In this thesis is shown that it was possible to produce porcelain ceramic slabs with embedded microchannel using Additive Manufacturing methods. The process developed is based on the combination of two additive manufacturing technique, namely the Layer-wise slurry deposition (LSD) of porcelain with the Direct ink writing (DIW) or Robocasting of graphite-based ink. Layer-wise slurry deposition is a technology for the deposition of highly packed powder layers by means of a doctor blade, this deposition technique was combined with the Robocasting technology for the printing of a graphite-based ink on the previous deposited porcelain layers. Covering the printed ink with subsequent LSD steps, green parts with built-in ink filaments were obtained, and, after firing and removing the graphite, porcelain ceramic slabs with built-in channels were produced.

The results proved that it was possible to build channels, with certain design freedom of the path, inside ceramic parts and that, despite the limits due to the quality of the channel structures, this technology has a good future potential and can be improved and adapted to be employed in the ceramic production with applications involving microchannel structures.

Riassunto esteso

Nel presente progetto di tesi vengono riportati risultati relativi allo studio di una nuova tecnologia basata sull'ibridizzazione di tecniche AM applicate ai materiali ceramici finalizzata alla produzione di ceramici funzionali con microcanali integrati.

Generalmente le parti in ceramica con microcanali sono realizzate aprendo dapprima i microcanali e poi ricoprendoli con ceramica aggiuntiva attraverso metodi di giunzione. Per l'apertura dei canali vengono generalmente utilizzate metodologie come la goffratura, la litografia di precisione e la lavorazione laser. Il metodo però più avanzato per la fabbricazione di microcanali all'interno di materiali ceramici è detto "Low-temperature cofired ceramics" (LTCC), il quale consiste nell'impilare nastri ceramici verdi laminati, modellati e cotti per ottenere un bulk con microcanali incorporati. La natura di tali processi è però complessa, a volte limitata e soprattutto costosa per qualsiasi impianto di produzione.

In questo lavoro di tesi viene descritto come è stato possibile produrre lastre ceramiche in porcellana con microcanali incorporati utilizzando un processo basato sulla combinazione di due tecniche di produzione additiva, ossia il "Layer-wise slurry deposition" (LSD) e la tecnologia Robocasting, anche conosciuta come Direct ink writing (DIW). LSD è una tecnologia per la deposizione di strati di polvere altamente imballati, in questo caso slurry di porcellana, per mezzo di un doctor blade. Come accennato, questa tecnica di deposizione è stata combinata con la tecnologia robocasting per lo stampaggio di un inchiostro a base di grafite sugli strati di porcellana precedentemente depositati. Ricoprendo l'inchiostro depositato con successivi strati di slurry sono state prodotte parti verdi con filamenti di inchiostro incorporato, che, dopo cottura e rimozione della grafite, hanno permesso di ottenere lastre in porcellana con canali integrati.

I risultati hanno dimostrato che è stato possibile costruire canali all'interno di parti ceramiche con una certa libertà di progettazione tipica dei processi AM. Nonostante i limiti dovuti alla qualità delle strutture dei microcanali, la tecnologia così pensata presenta un buon potenziale futuro e se migliorata e sviluppata potrebbe essere utilizzata nella produzione ceramica con applicazioni che coinvolgono strutture a microcanali.

Table of contents

Introduction

Functional ceramics materials are generally characterized as materials possessing particular intrinsic properties and functions. In addition to applications ranging from microelectronics to biomedical, ceramics are also suitable for applications in the manufacturing of microchannel structures widely used for fuel cell, heat exchangers and microfluidic devices.

Typically, the ceramic parts with embedded channels have been fabricated by first opening microchannels and then covering them with additional ceramics. These openings can be fabricated using several methods, such as mold embossing, lithography, and laser machining. After fabrication, the channels have to be covered using sealing or joining methods. Precision lithography and engraving technology used in the semiconductor industry are also supported by alternative techniques such as electroforming and stamping or replaced by the most advanced Low-temperature cofired ceramics technology. The nature of such processes is complex, limited and expensive for a manufacturing foundry.

This thesis reports the work carried out at BAM (Bundesanstalt für Materialforschung und -prüfung) from January to June 2019. The work aims to demonstrate the feasibility of a novel method for the fabrication of microchannels embedded in ceramic slabs. The process developed is based on the hybridization of two additive manufacturing technique, namely the Layer-wise slurry deposition (LSD) of porcelain and the Robocasting of graphite-based ink.

The first part of the work deals with the typical applications and construction methods for microchannel ceramic structures and the main AM technologies suited for ceramic materials, with a particular focus on the layer-wise slurry deposition and robocasting technologies.

The second part focuses on the materials characterization and the methods adopted in the present work. Analysis such as differential scanning calorimetry, thermogravimetry, XRD, hot stage microscopy, density and porosity measurement were performed for the physical characterization of materials. The rheological properties of the ink have been studied by rheometer tests. The description of the process optimization phases and the analysis of the results obtained, with an examination of the limitations and future improvements of the process conclude the thesis work.

Chapter 1: Microchannel structures engineering

Today are available several applications that utilize microchannel structures, which range from fuel cells to microreactors, from heat exchangers and heat sinks to microfluidic devices. This chapter describes the main applications and construction methods of this type of ceramic structures.

1.1   Ceramic micro-engineered reactors and heat exchangers

The term "microreactor" traditionally means a small tubular reactor for testing catalyst performance, but with the development of microfabrication technologies, this term generally refers to chemical systems manufactured using techniques originally developed for electronic circuits.

Such systems have feature sizes in the submillimeter range, this size reduction and integration of multiple functions can lead to the production of structures with higher capacities than conventional macroscopic systems. Klavs F. Jensen at al.[1] in his experiment demonstrated the advantages of chemical processes resulting from increased heat and mass transfer in small sizes with model gas, liquid and multiphase reaction systems.

The reactors are required to have large reaction surface, and work at high temperatures and under an oxidative/reducing environment. Microchannels can introduce a high surface area/volume ratio, thus, the ceramics with embedded microchannels are ideal for both high-temperature heat exchangers and microreactors.

Heat exchangers can be used to recover thermal energy and make the industrial processes more energy efficient. The more heat that can be recovered, the more efficient the process will be, so there is a strong demand for heat exchangers that operate at as high a temperature as possible. Microchannel heat exchangers and reactors can provide very high performance in small dimensions, these are typically fabricated from metal (aluminum, copper, stainless steel) and silicon materials. The working temperature limit of steels is typically around 850°C but usually the expected working temperature for the heat exchangers is higher, normally greater than 1100°C. In addition, the exhausted gas stream often contains corrosive components for the metal, such as oxygen, carbon, and sulfur with an increased corrosivity due to the high temperature.

Ceramic heat exchangers permit operation at higher temperatures than with other materials. Additionally, compact heat exchangers are highly efficient and cost-effective. Due to their thermal and chemical stabilities, also ceramic microchannel reactors can offer some significant advantages over their metallic counterparts, including very-high-temperature operation and corrosion resistance in aggressive chemical environments[2], low cost of materials and manufacturing, and compatibility with ceramic-supported catalysts. Danielle M. Murphy et al.[3] describe in his work a ceramic reactor with microchannels that, combining the functions of heat exchanger and reactor, allows to obtain a syngas with an efficiency of the heat exchanger close to 90%.

Thus, with fluids passing through the microchannels, mass and heat transfer rates are significantly improved compared to macrochannel structures due to the high surface area and the ceramics with embedded microchannels are ideal for both high temperature heat exchangers and microreactors

(a)   b)
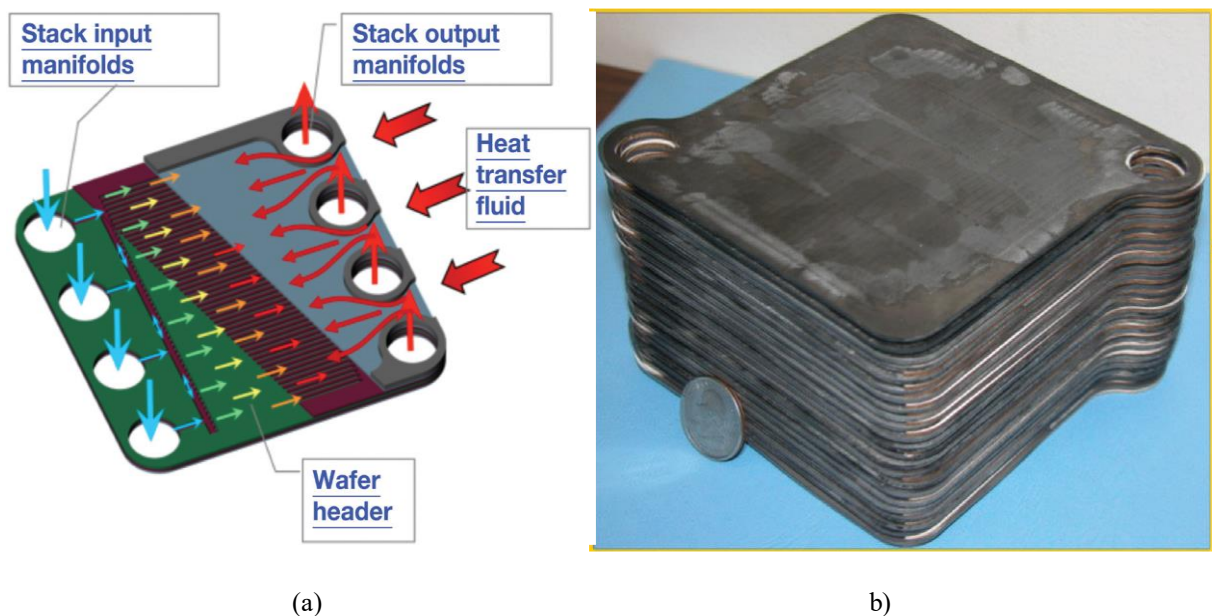
Figure 1.1. *a) Schematic design of a microchannel plate for a ceramic heat exchanger b) Example of a stack of silicon carbide heat exchanger plates.[4]*

1.2   Ceramic microfluidic devices

Microfabrication techniques have reached great advances in the electronics industry but are also used in different fields of chemistry and biological applications to realize structures with capabilities exceeding those of conventional macroscopic systems.

Microfluidics is the science of manipulating and controlling fluids in networks of channels with dimensions from tens to hundreds of micrometres. This discipline takes its origins in the early 1990's and has grown exponentially. In a microfluidic device, an object often with microchannels, fluid reactions, separations and/or detections occur. These devices generally work with nanoliters of reaction volumes and often fulfil the specific task in milliseconds of reaction and diffusion times. It is viewed as an essential tool for biology research, in a larger way in biotechnologies, chemistry, energy and pharmaceutics.

Microfluidic device materials initially consisted of silicon and glass substrates, while advanced materials were selected over time. These materials can be organized into three broad categories: inorganic, polymeric and paper. In addition to glass and silicon, inorganic materials such as low-temperature fired ceramics and vitroceramics have been introduced. Polymer-based materials include both elastomers and thermoplastics. Paper microfluidics is an emerging technology, the device are substantially different from those made from other materials.

Inorganic materials such as silicon, glass and ceramics are the most commonly used materials in microfluidics. The materials used, are also called *bulk materials* or *substrates* of the devices, function as the building blocks of various types of microfluidic devices

Generally, a microfluidic device can be built by first manufacturing open microchannels in a flat substrate using several methods (etching, mechanical machining, molding or casting) and then bonding this substrate to another flat plate forming a network of microchannels embedded in the bulk material, with the desired configuration and dimentions.
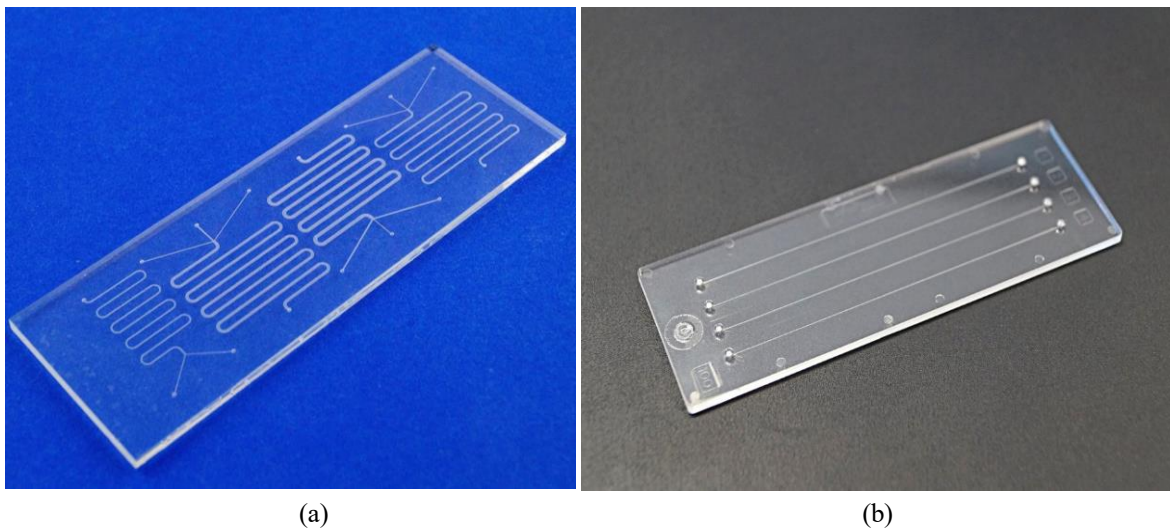

(a)   (b)

Fig.1.2. *Examples of microfluidic devices (chip) in glass (a) and polymer PMMA (b)*

1.3 Fabrication methods of embedded microchannels in ceramic materials

The need to produce functional micro-devices, in addition to industrial interests, has encouraged the sector towards research and development of new materials and technologies. The most advanced method of fabricating microchannels within ceramics is to stack laminated and patterned ceramic green tapes to obtain a bulk with built-in microchannels.

Low-temperature cofired ceramics technology (LTCC) has been pointed out to be the most suitable choice for a wide range of applications; microelectronic and microsystem applications[5], wireless[6] and biomedical microfluidic applications[7]. The material generally adopted is a ceramic based on aluminium oxide.

The most interesting properties for microfluidic device fabrication by LTCC are their excellent thermal and chemical stability and hermeticity. In the realisation of three-dimensional microfluidic structures, LTCC is superior to glass, silicon, polymethylmethacrylate, or polydimethysiloxane technology in terms of its quick production throughput and cost effectiveness.

The LTCC technology is based on simultaneous firing of tapes together with screen printed thick-film material at temperatures lower than those of conventional ceramics, usually lower than 900 °C[8]. To fabricate three-dimensional structures in multi-layer LTCC substrates, a multi layered thick-film sheets (individual green tapes) is first modelled to form holes, cavities, channels or other predetermined shapes. These individual green tapes are glued by uniaxial lamination, the tapes are pressed only in the direction perpendicular to the plane of the stacked tapes (z-direction) and then heated to form multi-layer laminates[9]. The deformation of the tapes occurs, in this way, mainly along the z direction.

Subsequently, this laminate is co-fired in a furnace in two stages. Firstly, a debinding stage in which solvent and organic binders are removed from the laminate during a heating treatment at ca. 500 °C. Then, the sintering stage during which the laminate is densified. After the co-firing process, a monolithic multilayer ceramic substrate containing three-dimensional structures is formed. A flow diagram of the LTCC manufacturing process for is presented in Figure 1.3.
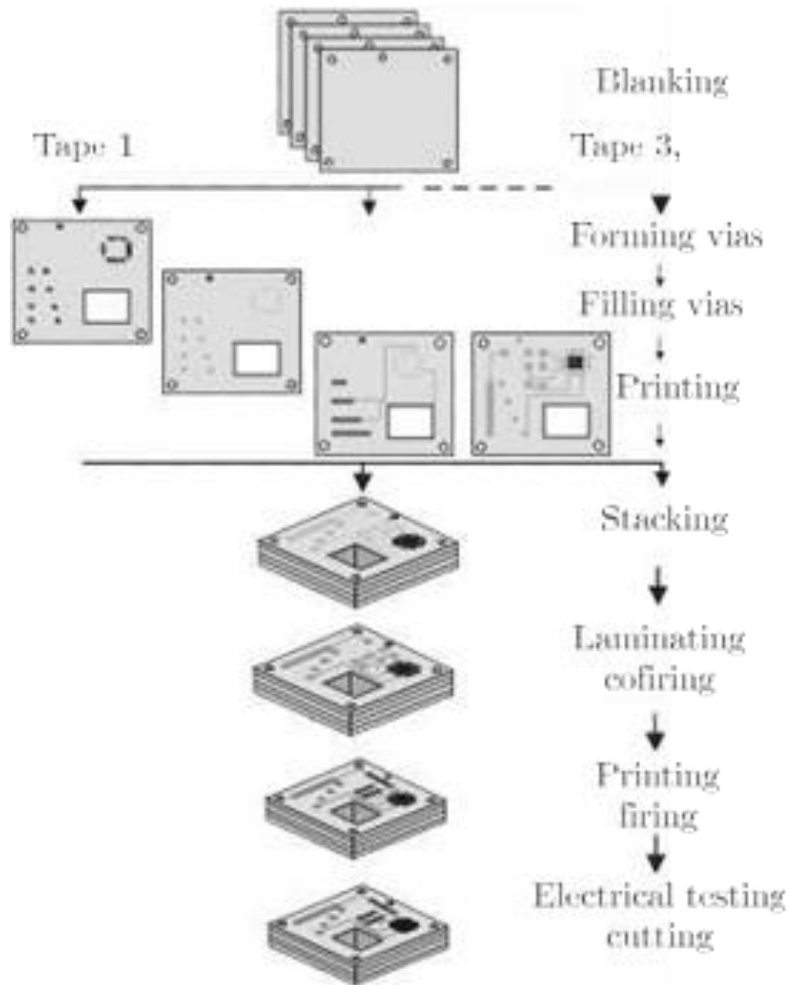
Figure 1.3. LTCC manufacturing process steps.

In spite of all the benefits previously listed, there is no lack of difficulties during the fabrication of micro-fluidic devices using the LTCC technology; during lamination and/or co-firing processes, these three-dimensional structures, especially suspended structures, tend to deform and sag[10]. In some cases, the microchannels collapsed and the layers around the microchannels suffered delamination[11].

Especially the glass content of the tape, used to increase densification at relatively low temperatures, may result in deformation of the suspended ceramic material due to softening of the glass component during the co-firing. This effect on the three-dimensional structure during firing is because of the glass softening temperature (*Tg*), at which viscosity reduces considerably and the glass is subjected to mechanical constraints exerted by the device features that usually leads to failure of structures such as microchannels, membranes etc. (sagging). This is in particular an important issue for production of object with critical dimensions. In addition, an excessively high glass content prevents the fabrication of many high-temperature or functional ceramics. Another problem is the alignment of multiple layers, that is also a challenge.

To date, the creation of complex or three-dimensional structures such as channels integrated in the ceramic material, with good dimensional stability and mechanical integrity, is laborious and under improvement. This thesis work aims to show an innovative simple method for fabricating three dimensional microchannels networks within ceramic material, combining different additive manufacturing processes.

Chapter 2: Additive Manufacturing of ceramics

Additive manufacturing (AM), also designated as solid freeform fabrication (SFF), rapid prototyping (RP) or more popularly called 3D printing, represent a family of technologies in which a part is directly generated from a virtual model, initially created using a three-dimensional Computer-Aided Design (3D CAD) system, by adding material layer-by-layer. AM is defined by ASTM F2792-12a as the "process of joining materials to make objects from 3D model data, usually layer upon layer, as opposed to subtractive manufacturing methodologies, such as traditional machining".[12] Differently from the other technologies that remove material from a bulk, using AM techniques 3D objects are built through a layer- by-layer approach by processing solid filament, liquid or powder stock materials. The material is in a state optimized for the layer deposition process. In this way it is possible to obtain parts with arbitrary geometries without the need to modify the typical production process.

All AM parts start from a software model, this can involve the use of almost any professional CAD solid modelling software, that describes the external geometry. Afterward the resulting 3D model is converted into a standard tessellation language (STL) file which describes the external closed surfaces of the original CAD model and provides the basis for calculation of the slices. According to the fabrication process, after removing the 3D build parts can need further finishing and cleaning processes.

The initial motivation for the development of RP technologies was to reduce the time to market of new products. The rapid character of this technology is due to the acceleration of the entire product development process which depends largely on the use of computers to reduce design, testing and implementation time. Recently, these technologies are used for more purposes, parts ready to use but also semi-finished parts can be obtained in an economically and technically way. Consequently, AM is receiving increasing interest from industry and society and when used in conjunction with other technologies to form process chains can significantly reduce product development times and costs.

There are also advantages in terms of the reduction in process steps. Building with an AM machine is generally performed in a single step while most other manufacturing processes would require multiple steps. Using conventional methods, a change in the design, even a relatively simple one can dramatically increase the number of these steps, resulting in increased building time Furthermore AM does not need special cutting tools, these processes are not constrained in the same way of machining tool so undercuts and internal features can be easily

built without specific process planning. This makes it possible to build up parts with complex shapes, so the higher is the geometric complexity, the greater the advantage AM has over other manufacturing processes. A further important advantage of producing parts by adding material is the more efficient use of raw material and the less waste production.

The development and research of this group of technologies started in 1980's, nowadays the development is advancing very fast and the physical properties of the parts generated are the main objective. Significant progress has been made, an entire set of AM technologies has been developed[13] and the expectation is that AM technologies can provide and improve benefits to the society, such as: healthcare products, reduction on the use of raw material, energy and consumption and on-demand manufacturing. According to ISO/ASTM 17296 standard on Additive Manufacturing Technologies[14], seven types of AM processes can be differentiated: material jetting, material extrusion, direct energy deposition, sheet lamination, binder jetting, powder bed fusion and vat photopolymerization. Polymeric, metallic, and ceramic materials can be all processed by these technologies, surely the technologies based on the processing of polymeric and metallic materials have been the most successful. These seven AM technologies can all be applied to shape ceramic components, mostly starting from submicrometer-sized ceramic powder particles[15].

The most successful AM technologies applied to ceramics have been used to fabricate porous structures, scaffolds for biological applications, filters etc. A further application particularly compatible with the use of many of today's AM technologies for ceramics is the production of filigree structures[16]. All these applications tolerate or even require a certain amount of residual porosity in the solid ceramic part. This is due to the reason that AM makes it possible to produce porous architectures with dimensional precision, complex shape and pores control not achievable with any other technology.

Generating instead dense monolithic ceramic bodies by AM is really complex and the development of a technology that allows monolithic components to retain their properties is still a challenge. Advanced ceramics are normally made of fine powder, these powders have a low flowability and are subject to agglomeration and electrical charge, so they do not pack well. Thus, the physico-chemical properties of advanced ceramics will not be excellent, as they depend directly on the microstructure, which is linked to the particle packaging and applied sintering heat treatment.

The seven types of AM processes mentioned above could be divided into basically two different categories (as shown in Figure 2.1) according to the ISO/ASTM standard:

(1) The direct processes (also called single-step step processes), in which parts are fabricated in a single operation where the basic geometrical shape and basic material properties of the

10

intended product are achieved simultaneously by means of the direct deposition of the material only in the position giving the desired shape of the final object.

(2) The indirect processes (also called multi-step processes), in which the parts are fabricated in two or more operations where the first typically provides the basic geometric shape by the deposition of a first layer of material and the following consolidates the part, the cross section (slice) of the part is inscribed in the layer and, after completing all layers to complete the process, excess material surrounding the part is removed to release the final object.

Before proceeding with the description of the main AM technologies, it is important to make some general considerations regarding the two categories of processes. The indirect processes require excess material which is, in any case, necessary to form a support to the next layers, allowing the generation of parts with large overhangs. On the other hand, it is necessary to remove the excess material at the end of the process, which may be difficult or impossible for some geometries. Direct techniques, instead, does not have such geometrical limitations, but requires support structures for large overhangs, which means more process time and the need to remove the support to get the final part.

Indirect technologies are generally faster, and the cross-section of the piece to be built, the layer, can be printed on the whole area. Moreover, the simultaneous fabrication of multiple individual parts can be achieved. On the other side the single step processes are ideal for multimaterial systems (ceramic/plastic or ceramic/metals), for the others this possibility is limited. Most of the AM processes to shape ceramics are indirect processes since they use of a binder material to selectively bond ceramic dust particles

Here there is an overview of the main additive manufacturing technologies of ceramics, more attention is certainly given to the technologies adopted in this work.
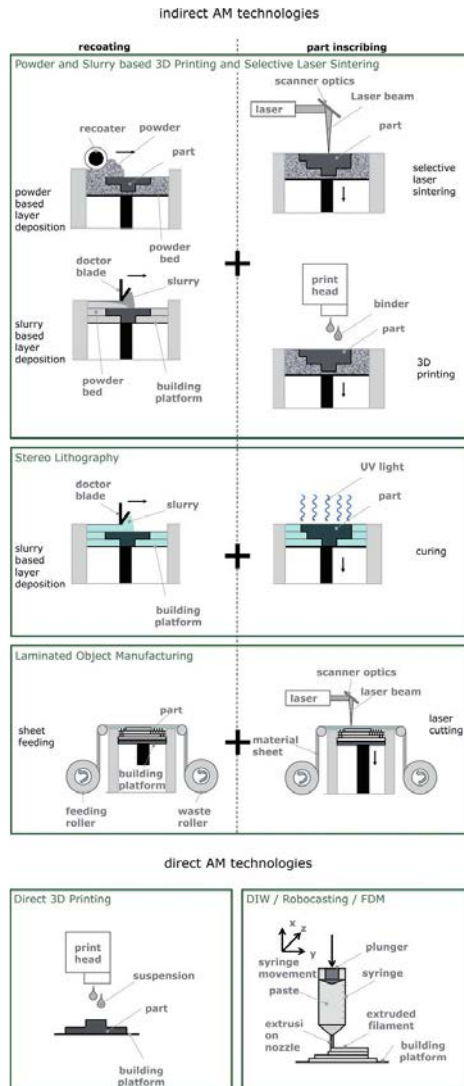
Figure 2.1. *Schematic of AM technologies[16].*

.

2.1 Indirect AM technologies of ceramics

The most common indirect technologies, described in the following paragraphs, are certainly Stereolitography, Laminated Object Manufacturing, Powder-Based sistems and their extensions Layer-wise slurry deposition-3DP (LSD- print) and Layer-wise slurry-laser sintering (LSD-SLS).

2.1.1 Stereolithography (SLA)

Stereolithography is the older AM technologies, developed in the mid-1980s. It is classified as a Vat photopolymerisation process which make use of liquid, radiation-curable resins, or photopolymers, as their primary materials. Vat photopolymerisation processes are defined as "additive manufacturing processes in which liquid photopolymer in a vat is selectively cured by light-activated polymerization"[14].

It uses a vat of liquid photopolymer resin cured using a process of photo polymerisation or UV light, where the light is directed across the surface of the resin with the use of motion controlled mirrors (Figure 2.2). A photosensitive polymer is cured or hardened (polymerise) by this UV light or a laser layer-by-layer. Once one layer is completed, the construction platform is vertically lowered to a given distance and a new uniform layer of resin is placed on the top of the previous solidified one.

In order to provide a smooth resin base to ensure that there are no defects in the resin for the construction of the next layer, some machines use a blade which moves between layers. The process continues and is repeated until the 3D object is completed.

The stereolithography of ceramics is based on the photopolymerization of a liquid resin filled with ceramic particles. Different ceramic-containing slurry layers are scanned by ultraviolet (UV) radiation which causes a chemical reaction that results in the polymerization of the slurry layers with incorporation of the ceramic particles. To obtain the final ceramic part is necessary the debinding of the polymer and the sintering of the structural material in a furnace.

The SLA process has a high level of accuracy and good finish but often requires support structures since the process uses liquid to form objects, so there is no structural support from the material during the build phase, unlike powder-based methods. Further actions include the removal of non-polymerised resin and the post-curing of the printed 3D part under UV light to make it strong enough for structural use. Considerable defects like the shrinkage of the structure during the production process, the necessity of a support, the presence of a toxic resin and long post-processing times limit the use of this technique.
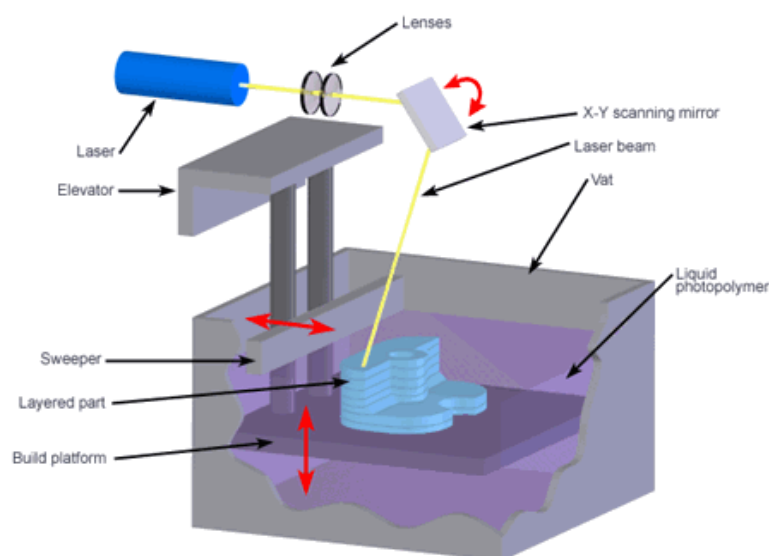

Figure 2.2. *Stereolithography apparatus (SLA).*

13

2.1.2 Laminated Object Manufacturing

In Laminated object manufacturing (LOM), parts are built by stacking layers of sheet feedstock material which is laser cut according to the tool path file. Paper, plastic and metal are generally used as sheet materials. As shown in Figure 6, after the first layer of a sheet material is loaded, a laser (CO_2 tipically) or a razor is used to tracks the cross section designed and, after the removing of the excess material, a second layer covers the previous one and again the laser traces the cross section following the information in the STL file. Each layer is bonded to the previous one using adhesives or welding techniques. The process is repeated several times until the desired 3D object is obtained.

Ceramic tapes are used as feedstock material in the LOM of ceramics. First the tapes are sprayed with a solvent, which acts as an adhesive, and then stacked to bond them together. The tape is then cut with a laser according to the file path. After laser cutting, a heated roller is used to further bond the tapes by thermo-compression. Finally, the part is released and removed manually.

To achieve optimum adhesion between sheets, a controlled heating phase is required during production, both on the stage and on the roller, to ensure that the adhesive acts to bond the sheets together. If the local temperature of either the roller or the stage is not controlled well enough, the inefficient adhesive heating could delaminate the part or induce structural damage. However, the non-uniformity effect of this process in the manufactured part is minimal compared to the defects observed in other AM techniques. Another restriction of the LOM is the limitation of the applicable materials, which are selected on the basis of their ability to be formed into sheets and to be integrated with the adhesive.
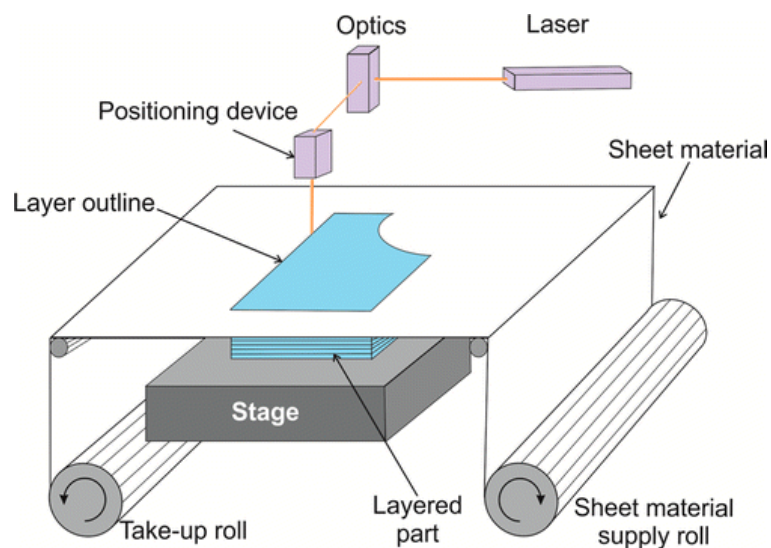

Figure 2.3. *Schematic of the LOM process.*

2.1.3 Binder Jetting (Powder-Based 3D Printing)

Also known as three-dimensional printing (3DP), developed in the early 1990s primarily at MIT, Binder Jetting (BJ) is an ink-jet printing technology in which a liquid bonding agent is selectively deposited to join powder particles. It's a Powder-based system, consisting of a printing head and a powder deposition device. Figure 2.4 shows the basic components of the 3D printer.

First the deposition device spread a layer of powder and then the printhead strategically drops binder into the powder[17], typically binder droplets form spherical agglomerates of liquid binder and powder particles as well as provide bonding to the previously printed layer. Once a layer is printed, the powder bed lowered (right piston) and a new layer of powder is spread into it (via a rolling mechanism). This process is repeated layer-by-layer until the part is completed. The printed part is typically left in the powder bed in order to fully set and to gain strength. Post-processing involves removing the part from the powder bed, removing unbound powder by pressurized air, and infiltrating the workpiece with an infiltrant to improve its strength and other mechanical properties.

The BJ parts are self-supporting in the powder bed so that support structures are not needed. Similar to other powder-based processes, multiple parts can be produced simultaneously in the powder bed. BJ process does not require high energy, does not involve lasers, and is relatively inexpensive. However, appropriate binder and material selection, optimization of the processes (e.g. layer thickness, powder packing density, wettability, flowability as well as binder drop volume) and removal of the loose powder after printing are important features to consider for obtain a good quality printed part. Thus, the major shortcomings of the powder-based 3D printing technique is that for any new powder-based material the optimization process may require a long time.

Binder jetting is considered the traditional method to produce ceramic parts by means of 3D printing, a wide range of ceramic materials has been developed for BJ by researchers. Liquid binders are the most versatile solutions as they work with almost all materials, however, in the case of organic binders, they can dry in the printhead, causing the nozzle to become blocked. An alternative is the use of an in-bed binder: a powder-based component is added to the initial formulation which binds the particles after interaction with a sprayed liquid. This technique achieves a higher strength of the green body than liquid binders.

Green parts created by BJ process are subjected to a thermal decomposition to remove the polymer binder and subsequently sintering of the part. Sintering is the most important phase of post-processing, which provides greater mechanical strength to the 3D printed object.

Powder-based 3D printing is particularly recommended for the production of large parts if the printheads consist of thousands of jets working in parallel. Multiple nozzles can also be used to cover a wide printing area and could be used to fabricate ceramic objects for architectural applications[16].

Most of the ceramic applications of this technology currently concern the shaping of porous biomedical scaffolds for tissue engineering. Main advantages are the customization of the parts, the control of the porosity and the absence of contamination due to toxic solvents, important elements in the realization of medical devices.

On the other side, the low powder packing of the powder bed (<25% TD) results in low density and stability of the parts during the building process, moreover the part not provide sufficient sintering activity to form dense ceramics. For these reasons, is really difficult to produce ceramic monolithic component without residual microporosity by this technique.
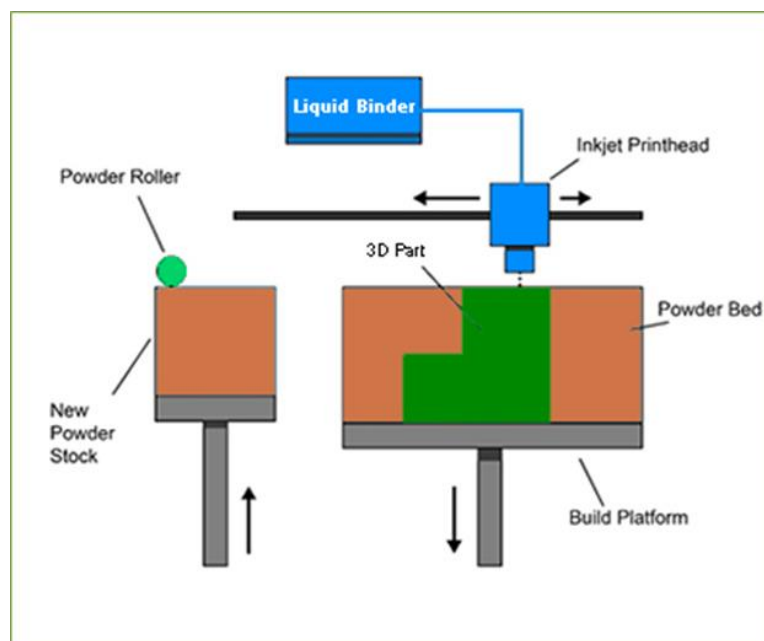
Figure 2.4. *Schematic setting of a powder based-3D printer*

2.1.4 Selective Laser Sintering (Powder Based Selective Laser Sintering)

Selective laser sintering (SLS) is classified as a Power-Bed fusion process, more precisely is a powder-based layer-additive manufacturing process in which a high intensity laser beam either in continuous or pulse mode is used as a heat source for scanning and selectively sinters regions of powder-based material placed in a powder bed.

The aim is to join powders in predetermined sizes and shapes of layers. The geometry of the scanned layers corresponds to the various cross sections of the computer-aided design (CAD) models or STL files of the object. After the first layer is scanned, the powder bed is vertically lowered by one layer thickness and the new layer of powder is spread mechanically by a roller on the top of the previous one. In this technology, the non-sintered powder serves as support for the build-up of the next layers.

A wide range of materials have been used in SLS, include wax, cermet, ceramics, nylon/glass composite, metal-polymer powders, metals, alloys or steels and polymers[18]. There are two types of SLS: the direct and the indirect one. In direct SLS, powders are just melted and consolidated by the laser, in indirect SLS, the densification of the powder is obtained by mixing powder with a binder phase. In this case only a binder material is melted by the laser, it should have a low-melting-point in order to serve as a glue. In this case the joining of the powders is caused by melting one of the low-melting-point components of the powder creating what is known as "green part. In both cases post-processing is carry out to improves structural integrity, mechanical properties, and decreases porosity. Further heat treatments are required to sinter the powders and consolidate the structure.

Direct laser sintering of ceramics is complicated by the poor resistance of this class of materials to thermal shock, moreover the sintering takes place in a short time interval (milliseconds), insufficient for binding to take place due to solid-state diffusion, leading to poor sintering of the ceramic material. Good results are obtained in the production of ceramic scaffolds with a good percentage of porosity, as well as for the P-3DP technology.
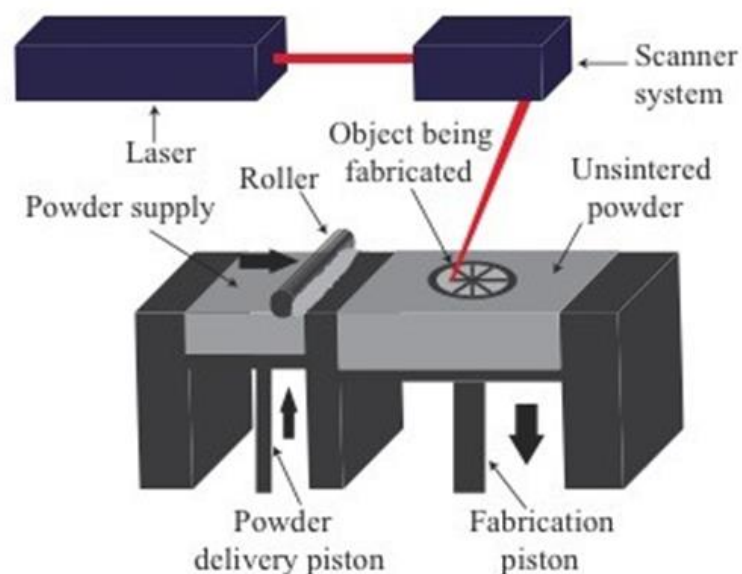

Fig.2.5. *Schematic setting of a SLS process.*

2.1.5 Layer-wise Slurry Deposition

As mentioned before in the powder-bed techniques the powder to be sintered is spread to a thin layer as a dry powder by means usually of a roller system. These layers have a relatively low density and for the manufacture of ceramics the formation of layers by deposition of a fine (< 30 μm) dry powder typically achieves a packing density below 50 % T.D. (theoretical density). The low powder packing results in a not sufficient density of the green part to obtain a full densification in the following sintering step.

Layer-wise slurry deposition (LSD) process is a logical extension of powder-bed technologies. In the LSD process, instead of dry powder, a ceramic slurry (liquid suspension of ceramic particles) is adopted to increase the powder packing density in the powder bed, in order to improve the sintering characteristics of the green part. Moreover, it can be possible to process finer powders by this method.

This LSD process combines elements from the tape casting and the slip casting processes (Figure 2.6). As in the tape casting process, a doctor blade spreads the ceramic slurry as a thin layer while, similar to slip casting, the layer formed adheres to the porous support. In this case, the porous support is the previous deposited and dried layers.
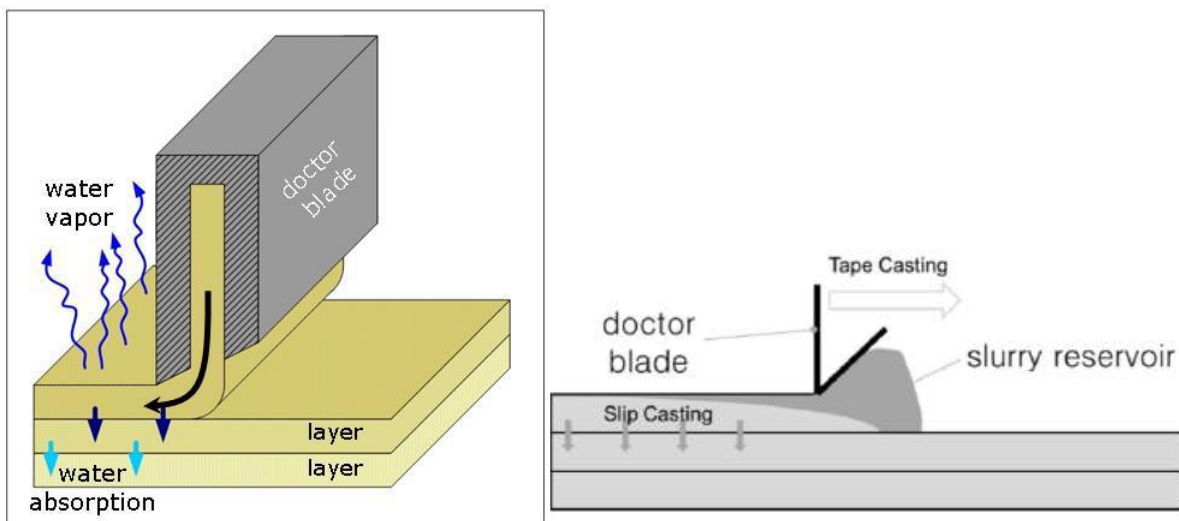
Figure 2.6. *Schematic of the LSD process[19]. Layers of a ceramic powder are deposited in a tape casting way using a doctor blade. On the right is shown the combination of the tape and slip casting processes that take place in the process.*

In the slip casting process, the slip is carried in contact with a porous body, the casting mold. When the slip is wetting the casting mold, the capillary forces drag the liquid phase of the suspension into the casting porous mold. The particles begin to compact forming a cast on the

surface of the porous mold. In the Layer-wise slurry deposition, as soon as the slurry touches the previously deposited layer capillary forces draw the liquid phase of the slurry into the pores of the previous layer and the formation of the cast begins.

The particle settling is dominated by several forces acting on each particle. The gravity force (Fg), which depends on the mass of the single ceramic particle, interparticle force (Fpp), and the inducted force *(Fd)*, which is the force inducted by the flow field into the dried porous layer, acting as shown in Figure 2.7. The buoyancy *(Ff)* is important in suspensions so must also be taken into account.

In the case of AM processes using dry dust, instead, the flow of particles in the layer deposition process is dominated only by gravitational and interparticle force. For the smaller particles, the force between the particles is dominant in relation to the gravitational force, the first depending on the particles surface and the second on the mass of the particles. This is why small particles do not pack well when freely settled. Slurries facilitate the use of fine powders, size range *>100 nm to <100 μm.* Moreover, mobility of particles within the slurry allows their free settling faciliting a better powder packing.

The LSD mechanism described before provides a high powder packing density, which is in the range of 55 – 70 % T.D, depending on the material system used. Powder beds generated by LSD show a final green density similar to parts prepared by conventional slip casting.
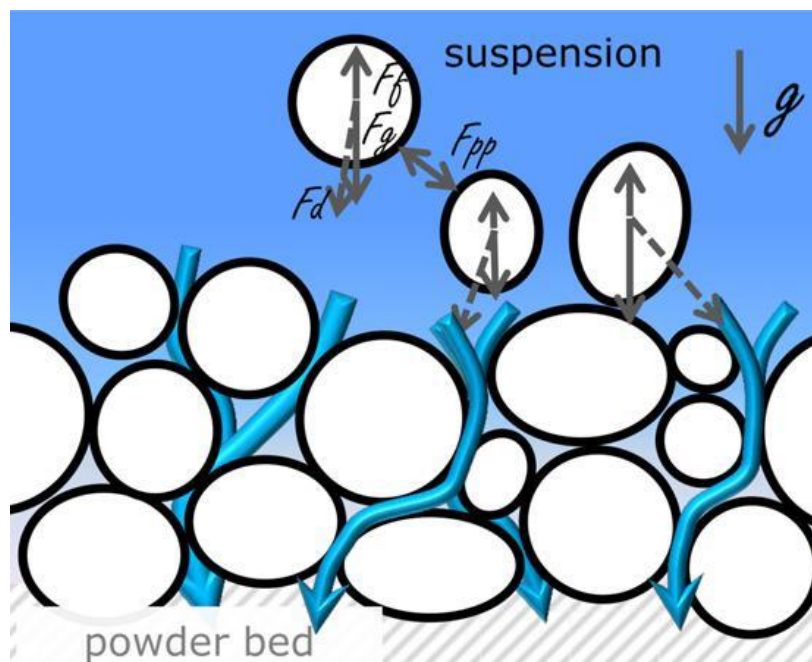

Figure 2.7. *Illustration of forces acting on each individual particle into the dried layer during layer deposition.*

The dimensions of the layers are defined by the characteristics of the system used. The width of the layers is defined by the width of the doctor blade in use, while the length is controlled by the movement of the blade parallel to the supporting surface. Thus, the width of the doctor blade and the trajectory of its movement determine the area of material deposition. The height is simply the sum of all the layers deposited, the typical thickness of the layers is about 100 μm.

An important parameter is the doctor blade speed, which must be high enough to prevent collision of the cast with the doctor blade (scratches), but, at the same time, a too high speed of the blade would cause an inhomogeneous deposition due to shear stresses within the suspension. Hence, it is important to adopt a correct blade speed during the deposition process.

The LSD process can generate two main defects: cracks upon drying and scratches. The smaller the size of the ceramic particles, the more likely it is that these defects will occur. The cracks can be generated by a differential shrinkage or by a constrained shrinkage. During drying of the cast layer, additional capillary forces are generated which lead to further shrinkage. While in slip casting this shrinkage helps to detach the cast from the mould, in LSD each layer strongly adheres to the previous one and for this reason shrinkage is limited in the layer plane (XY direction) and can only occur in the direction of layer stacking (Z direction). The constrained shrinkage in XY leads to biaxial stresses in the layer, which, depending on the amount of stress and the resistance of the layer itself, can create cracking.

Chiu et al.[20] studied and measured critical cracking thickness (CCT) in different systems. The study proved that cracks nucleate not only from trapped air bubbles, but also in apparently defect-free regions. In addition, it shows that CCT is independent of drying rate and increases with particle size. Cracking will not occur unless the energy required to form a crack is less than the energy gained in release the strain in the film.

From the relation (2.1) it can be observed that CCT *(h$_c$)* is a function of the biaxial stress *(σ)* developed in the film during drying and the fracture toughness *(k$_c$)* of the material.

$$(h_c = \frac{kc}{1.4 \times \sigma})^2 \tag{2.1}$$

Stress in a drying granular film is due to capillary pressure in the porous liquid, therefore, from the previous equation the critical thickness CCT will depend only on the capillary stress and the fracture resistance of the film[21].

The scratches are a defect which may occur during the process of the slurry deposition, they are the result of a collision between the doctor blade and the forming cast that occurs when the speed of the doctor blade is not sufficient. The spreading mechanism is shown in Figure 2.8: the doctor blade pushes a pool of wet slurry and as mentioned the cast starts to grow as soon as the slurry comes into contact with the porous substrate (previous dried layer).
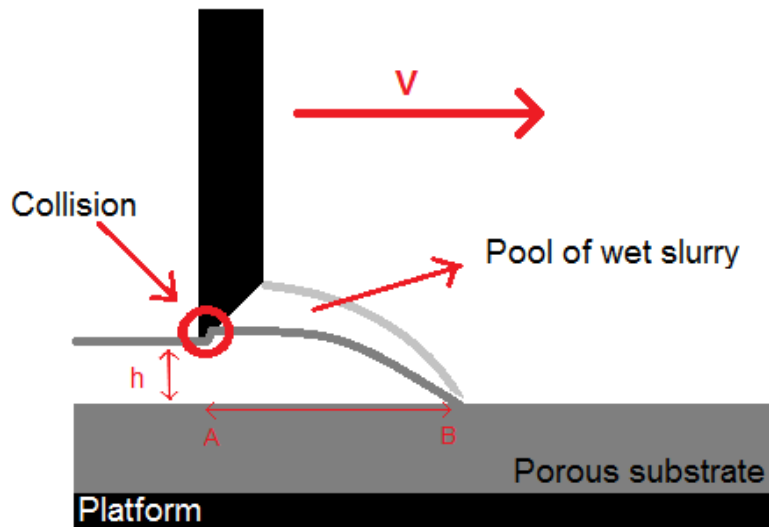
Figure 2.8. *Formation of the scratches after collision between blade and cast.*

The collision will occur if during the movement of the blade from A to B the cast grows to a thickness higher than h, where h is the distance between the doctor blade and the porous substrate. To avoid this, a sufficient speed of movement of the doctor blade must be maintained, which will be greater as the distance h decreases.

It is possible to obtain 3D parts combining the LSD process just described with binder jetting or laser sintering technologies. The parts are built following some steps: slurry preparation, layer deposition and drying, laser sintering or printing and finally cleaning and release of the part (Figure 2.9).
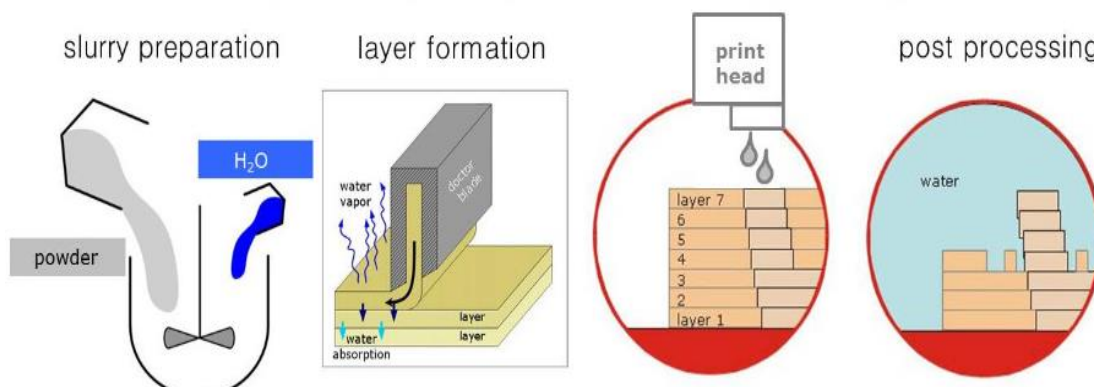
Figure 2.9. *Schematic illustration of the additive manufacturing process based on binder jetting with slurry deposition (LSD-Print)[22]. Step 1: Slurry preparation. Step 2: Layers of a ceramic powder are deposited using a doctor blade. Step 3: Each deposited and dried layer is locally binded by a print head. Step 4: The post processing consists in dissolving the non-sintered part in a solvent (water) in order to release the sintered body.*

Differently from the powder-based methods, the printed body obtained by LSD-print technology is embedded in a block of densely packed particles, therefore the release of the part must be achieved by dissolving the part in a solvent. In case of water-based slurries used for the layer deposition, water can act as a solvent for the powder bed. In this case, is important that the powder layers are dispersible in water, while the printed part must be non-dispersible in water and stronger than the surrounding powder.

The LSD printing process offers high potential for the additive manufacture of medium to large ceramic parts with high productivity. Lima P. et al.[23] showed in his work that the LSD-print process can be used as a novel Additive Manufacturing process for the shaping of porcelain samples with complex geometry, good detail resolution and surface finish (Figure 2.10).

As regards the LSD-laser sintering technology, a fundamental issue concerns the drying of the deposited layers because of the explosive vapour formation that can occur during the laser treatment of the layers due to the presence of residual solvent. For water-based slurries, it has been demonstrated that it only takes 10 seconds to dry a freshly deposited layer[24]. The drying process is related to two major mechanisms. First, as reported above, the capillary force drawn the solvent in the powder compact formed by the previous deposited layers and second, the temperature of the powder compact kept above the boiling point of the solvent system facilitating its evaporation.

Layer-wise slurry deposition was the technique adopted in this project to store layers of porcelain in order to obtain a ceramic compact part.

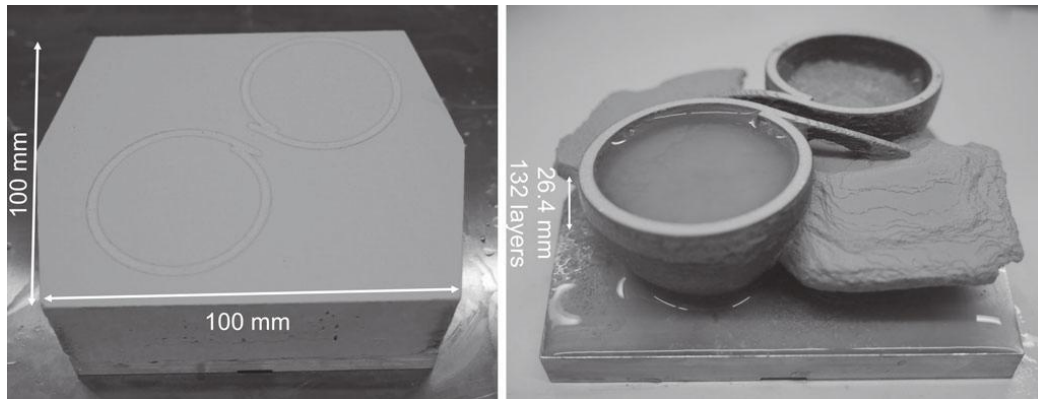**Figure 2.10.** Example of LSD-printed porcelain samples[23].

Figure 2.11. *Example of two cups made of porcelain by Layerwise Slurry Deposition-Laser sintering technology[25] (a) powder bed, formed by 132 layers with a thickness of 200 μm, containing the two laser-sintered cups; (b) cups partially released from the powder bed.*

2.2 Direct AM technologies of ceramics

Direct process means that the material is directly deposited to give the desired shape of the ceramic part. Direct AM technologies are material extrusion or jetting processes in which droplets of build material are selectively deposited or dispensed through a nozzle or orifice to shape macroscopic ceramic object[14].

2.2.1 Direct Inkjet Printing (DIP)

Direct inkjet printing (DIP) is a technology that uses a ceramic suspension to build structures through the subsequent deposition of individual drops provided by a printhead on a substrate, according to cross-sections of a three-dimensional model in order to build the final object with controllable geometry and composition.

Ceramic suspension, or ink, is made up typically of less than 30% of ceramic particles, dispersed in a liquid medium. Water or organic liquids can be used as liquid carrier, depending on the specific needs of the print head. Various additives are used to stabilize the suspension, adjust its viscosity and surface tension, and to control the spreading and drying of deposited droplets. On contact with the substrate, the droplets undergo a phase change shaping a solid part.

DIP builds the object directly from the material supplied by the ink, the complex ceramic structures generated by this technology show a high powder packing density which allow to obtain parts with appreciable mechanical properties.

2.2.2 Fused Deposition Modeling (FDM)

A fused deposition modeling (FDM) machine melts a plastic filament and extrudes it through a nozzle. The molten material is deposited on the construction platform layer by layer, each layer deposited on the platform cools and solidifies, in this way the part is built (Figure 2.12).

Fused deposition of ceramics (FDC) is a solid free-form fabrication technique based on the fused deposition modeling (FDM) involving the extrusion through a nozzle of a viscous ceramic paste in the form of a filament. The ceramic particles are first dispersed densely (up to 60 vol%) in a thermoplastic or wax filament. The filament is fed through a pair of counter-rotating rollers into a "heated liquefactor". Then layer after layer, the flexible filament is partially melted and extruded from a mobile head in the X-Y plane onto a Z stage platform to fabricate the green part.
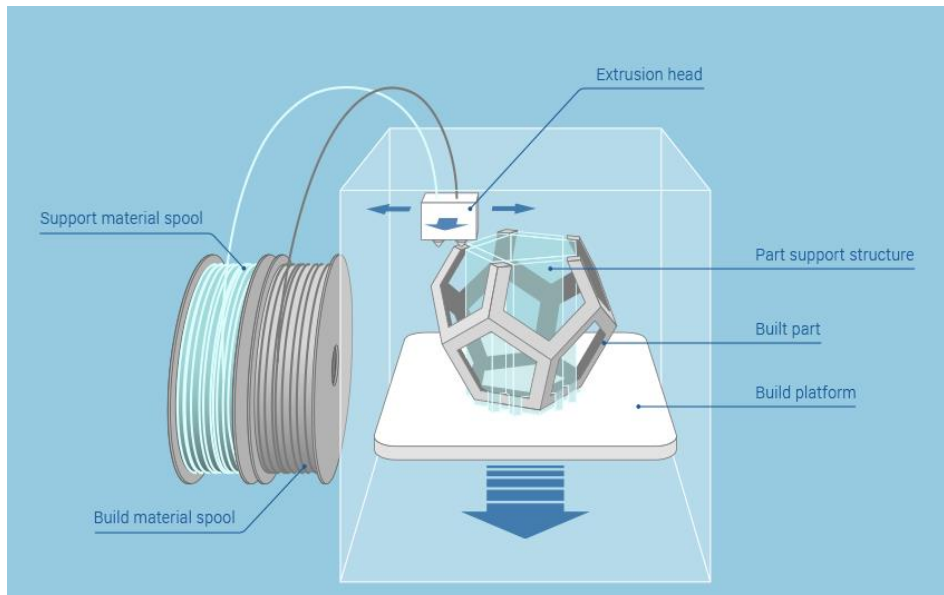

Figure 2.12. Fused deposition modeling process[26].

The filament acts both as a piston that guides the extrusion process and as a raw material for the process. The pressure drop required to extrude the material through the FDC nozzle depends on the viscosity of the raw material, the geometry of the nozzle, and the volumetric flow rate. If this pressure exceeds the critical load per unit of filament surface area, buckling occurs and the process is interrupted. The control of the rheological properties of the filament is essential to prevent deformation of the workpiece after extrusion and failure of the filaments.

Fused deposition modeling requires support structures that anchor the parts to the construction platform and make it possible to build the overhanging structures. If necessary, the support

structure can be made of a different material by using a second nozzle. It is possible to produce several parts at the same time, provided that they are all anchored to the platform. A limitation of this process is due to the fact that through the deposition of extruded material layer-by-layer the surface has a step-structure and fine details cannot be realized.

2.2.3 Robocasting (Direct Ink Writing)

Robocasting or Direct Ink Writing (DIW) is defined as additive manufacturing technology based on the direct extrusion of slurry-based inks on a surface, which contain the basic material that builds the desired structure without any further tooling. The technique was first developed by Cesarano J. at Sandia National Laboratories in 1996 for the freeform fabrication of ceramics and composites, under the name of Robocasting. This technique is defined by Cesarano J.[27] as "a freeform fabrication technique for dense ceramics and composites that is based on layer-wise deposition of highly loaded colloidal slurries".

In Robocasting a highly concentrated (~35-50 vol.%) colloidal suspensions of ceramic powders (< 1% of organic additives) in a solvent (water typically), is extruded through a nozzle to form a filament that is directly deposited to assemble three-dimensional structures in a layer-by-layer sequence. The ink must have important viscoelastic properties and, in general, a robocasting ink must meet two criteria:

1) it must be pseudoplastic enough to flow through a small deposition nozzle at modest shear rates without clogging (low viscosity under stress).
2) it must have an excellent shape retention capacity in order to maintain its shape under the load of overlaying layers (high elastic/storage modulus, and high yield stress).

The pseudoplastic ink flows and turns into a pseudo-solid mass after deposition. The retention of the shape, unlike other freeform fabrication techniques, does not require solidification or reactions but is based only on the rheology of the ink deposited and partial drying of the individual layers. In practice, the ink behaves like a viscous gel when loaded into the printhead, while during extrusion the shear stress breaks the gel structure and the viscosity decreases significantly. After extrusion, the fluid undergoes a rapid gelling process that increase the viscosity back to a level comparable to before extrusion which prevents deformation of the filament. This behaviour can be obtained by a careful preparation of the colloidal ink, which first involves the preparation of a low viscosity but concentrated suspension, and subsequently the induction of a drastic rheological change, by changing the pH, adding salts or additives, etc., to obtain a gel or paste system with optimal rheological properties.

After preparation, the ink is normally extruded through a conical/cylindrical nozzle (typical range 100-1000 µm) from the computer-controlled robotic deposition system (Figure 2.13). The movement of the nozzle follows the CAD model previously designed by building layer by layer the desired part. The ink flows through the nozzle at the volumetric flow rate necessary to keep the linear deposition speed constant, lower speeds allow better shapes to be obtained at the expense of longer process times. After assembly, the green sample is typically dried under environmental conditions and heat treated for debinding and sintering of the ceramic part.

Usually in robocasting the ceramic suspension with a high solid load undergoes a transition from a pseudoplastic behavior to a dilatant behavior when extruded in air, also the drying involves clogging of the nozzle when it has a diameter greater than 500 µm.

To avoid this problem and to ensure uniform drying of the structure during assembly, the deposition process can be carried out in an oil bath (usually paraffin oil) as shown in Figure 2.13., or in a humid environment.
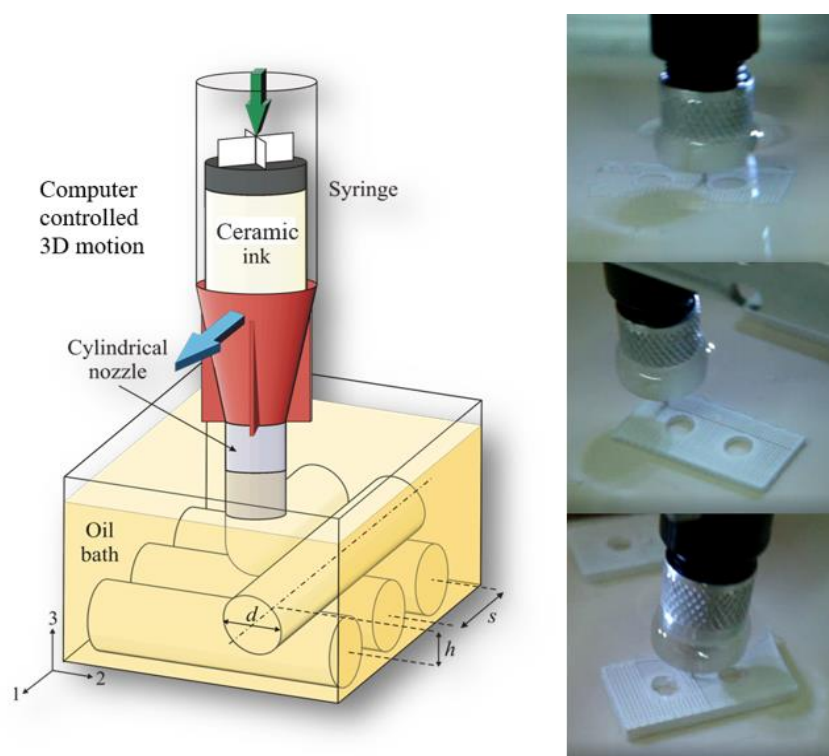

Figure 2.13. *Schematic illustration and images of the robocasting process within an oil bath[28].*

One of the main advantages of this technique is the lack of a powder bed, which allows to build 3D structures using minimal amounts of material, minimizing waste and avoiding further processes for the reuse of the surplus powders. The use of a ceramic suspension with high solid

load, in addition enables the production of bulk samples with high initial green densities, typically higher than 50% of the theoretical density of the material, which allows to obtain an almost complete densification after sintering.

Furthermore, self-supporting capacity of the robocasting inks and their high storage modulus allows the creation of porous structures and complex shapes without the use of moulds or support materials. DIW is therefore a particularly useful technique for the realization of porous structures used as catalyst supports, filters, and especially scaffolds for tissue engineering or other biomedical applications[29]. Scaffolds produced by DIW/Robocasting generally have better mechanical properties than those produced by powder-based technologies[16].

On the other hand, sometimes to create large overhanging features or complex parts, the use of a secondary support structure is inevitable to guarantee the correct assembly of a designed object. In this case, a secondary printing system and an additional ink in sacrificial material will be required, as shown in Figure 2.14. In the present work the Robocasting technique has been used to deposit graphite-based ink with sacrificial function in order to obtain embedded channels in a bulk ceramic material, as explained in the next chapters.
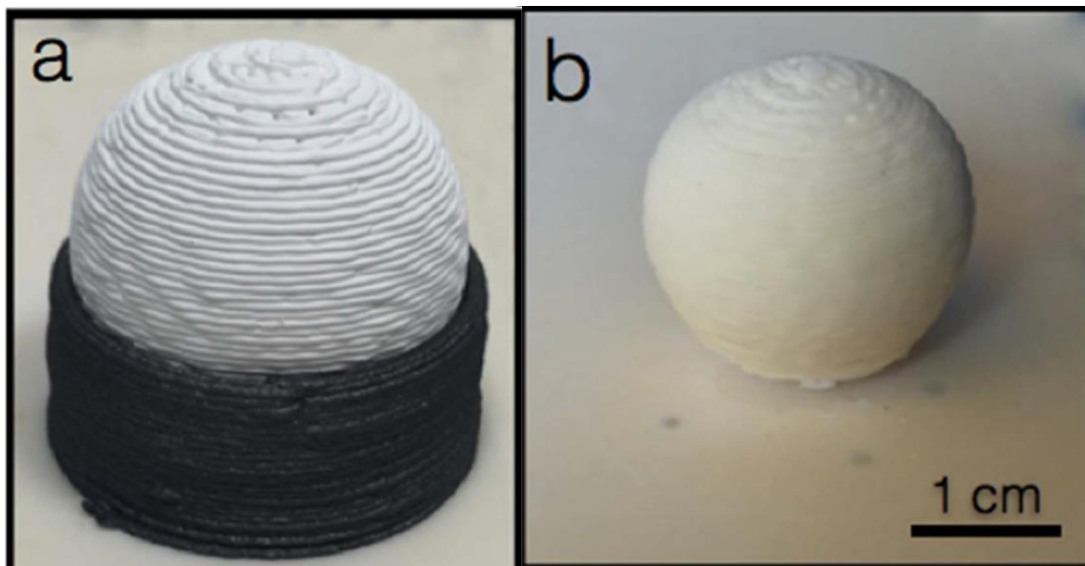

Figure 2.14. *Images of an alumina sphere assembled by robocasting using graphite ink as a fugitive support: a) as-printed; b) after burn-out and sintering, the graphite has been removed[30].*

Chapter 3: Materials and Methods

The focus of this thesis project was to combine 3D printing technologies as LSD and DIW/Robocasting techniques to build channels embedded into porcelain laminate. The process combined the deposition of porcelain slurry layers, followed by drying, with printing of a sacrificial graphite-based ink inside of channels previously dug into the layers in order to obtain a ceramic laminate having enclosed channels. The material used and characterized in the present work were a porcelain-based slurry, adopted for the LSD process, and a PPG-graphite based ink for the Robocasting process.

3.1   Porcelain Slurry

Based on ASTM Designation C 242 Porcelain is defined as a "glazed or unglazed vitreous ceramic whiteware made by the porcelain process, and used for technical purposes, designating such products as electrical, chemical, mechanical, structural, and thermal wares when they are vitreous[31]". Porcelain is probably the most known traditional ceramic materials but also one of the most complex. Composed mainly of clay, feldspar and quartz, porcelain forms a mixture of glass and crystalline phases after heat treatment. Variations in composition, nature of raw materials and firing temperature provide a variety of household (tableware, sanitary ware) or technical (chemical or electrical) quality products[32].

The porcelain slurry adopted was a suspension of porcelain particles in water (ca. 40% in volume), with a slight addition of additives. The slurry used in the process was characterized by means of particle size distribution and its theoretical density was measured by gas Pycnometer while phase quantification was performed by XRD analysis. The slurry was found composed of quartz, mullite, Kaolinite and Albite.

In order to optimize the firing condition, DTA and Hot Stage Microscopy analysis have been carried out, while after sintering the density and the porosity of the porcelain samples were measured by Archimedes method.

Finally, green, sintered and samples with built-in channel were observed by optical and digital microscopy and also studied by X-ray computer tomography analysis.

3.1.1 Particle size analysis

A sample of slurry was characterized by means of particle size distribution. Particle size analysis is useful for characterise the size distribution of particles in a sample, and it is applicable to solid materials, suspension and even aerosols. In this case a suspension of powder from the dried slurry mixed with a solution of *0,003molNa4P2O7* was used. The details of the system were range lens: 300 mm, beam length: 2.40 mm and obscuration:16.5%.

There are different methods for measuring particle size and it is important to select the most suitable method for different samples, since different methods can produce different results for the same material. The Mastersizer S (Malvern, UK) was used to obtain the distribution curves. This device uses a common particle sizing method, the laser diffraction. Laser diffraction is particularly used for particles between 0.5 and 1000 microns in size. The working principle is based on the diffusion of a beam of light (or laser) by particles, the scattering angle of light is inversely proportional to the size of the particles (Figure 3.1). It is surely a very fast, reliable and reproducible technique and can measure over a very wide range of sizes.

The powder, in this case wet, is carried by a stream that flows in front of a light, which makes the shadows of the particles appear on the other side, where there is a sensor. Based on the size of the shadows, the machine estimates the size of the particles and, if there are, agglomerates.
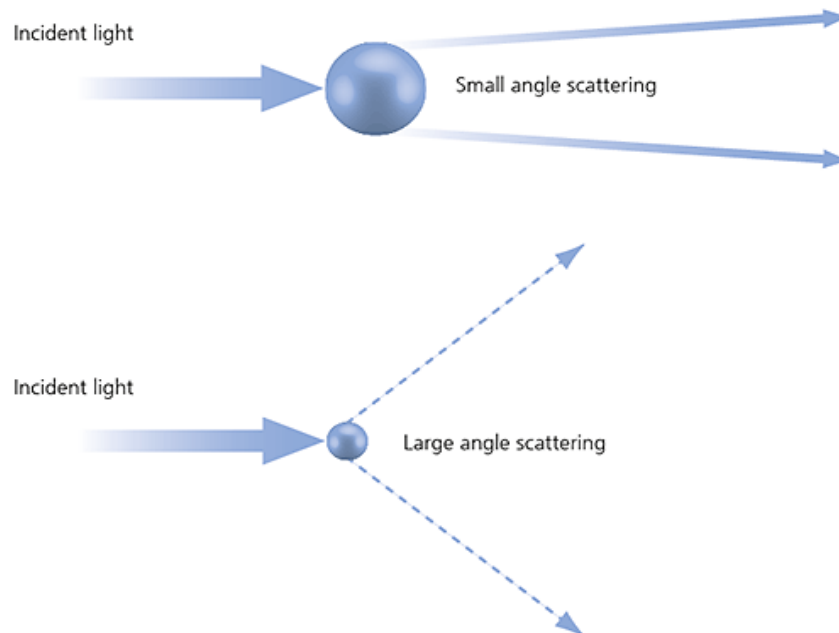

Figure 3.1. *Laser diffraction theory, scattering of light from small and large particles[33].*

3.1.2 Thermogravimetric and Differential thermal analysis

Differential thermal analysis (DTA) has been carried out to investigate phase transformation occurring during the heating of the porcelain-based slurry and optimize the sintering temperature.

In DTA, thermal effects on a material are observed during programmed thermal cycles. DTA is defined by ICTAC (International Confederation for Thermal Analysis and Calorimetry) as "a technique in which the difference in temperature between the sample and a reference material is monitored against time or temperature while the temperature of the sample, in a specified atmosphere, is programmed." During the test the sample and the reference are placed symmetrically in the furnace, an AlO_2 sample was used in the current test. The reference material must not present thermal events in the temperature range of interest and ideally should be a substance with the same thermal mass as the sample. The sample and reference temperatures are changed during this process, a thermocouple on the sample and a differential thermocouple on both the materials are set to detect the temperature difference between the sample and the reference. The temperature should be the same until thermal event occurs, such as melting, decomposition or change in the crystal structure.

The temperature difference (ΔT) is then plotted against time, either against temperature to obtain DTA curve. The ΔT is plotted on the y axis, while time or temperature on the x. In this way the temperature in which the sample absorb or released heat can be found (endothermic or exothermic reactions). If an endothermic event occurs within the sample, the temperature of the sample will be lower than the reference temperature and a minimum temperature will be observed on the curve. If an exothermic event occurs, on the contrary a maximum will be observed on the curve. The DTA can provide information regarding the sample transition and reaction temperature, but also on the nature of the thermal event.

Thermogravimetric analysis (TG) is a technique in which the mass of a substance is monitored as a function of temperature or time during a controlled temperature program in a controlled atmosphere. The result of a thermogravimetric analysis is a plot of mass as a function of time or temperature. This technique is used to measures mass change in a sample and investigate the causes related to it, such as decomposition, evaporation or oxidation.

3.1.3 Hot stage microscopy

In order to observe the shrinkage and the initial sintering and densification temperature of the green LSD samples, densification curves at temperatures between 1000 and 1300 °C with same heating rate were obtained by hot stage microscopy (Hesse-Instruments, Osterode am Harz,

Germany). The heating rate of the processes was 2°C/min until 500°C and 10 °C/min until the maximum temperature, isothermal dwell time of 5h.

The hot stage microscopy (HSM), is the combination of microscopy and thermal analysis to allow the study of materials as a function of temperature and time. Hot microscopy offers the opportunity to visually follow thermal changes, since it allows to observe and record changes in the samples contours with temperature, as shown in Figure 3.2. During the heating process there is a light on one side of the firing chamber that creates a shadow on the surface of the sample, a camera on the other side of the oven records any small variations in the shadow area. When the area starts to shrink, it indicates a sintering principle.

The visual examination allows to obtain important information about the material during heating, and in the production of glass and ceramics, HSM is used in particular to study the characteristic temperatures of softening, melting, flowing and sintering. HSM, moreover, permits to obtain useful sintering curves that present the ratio between the area % and the increasing temperature of the process.
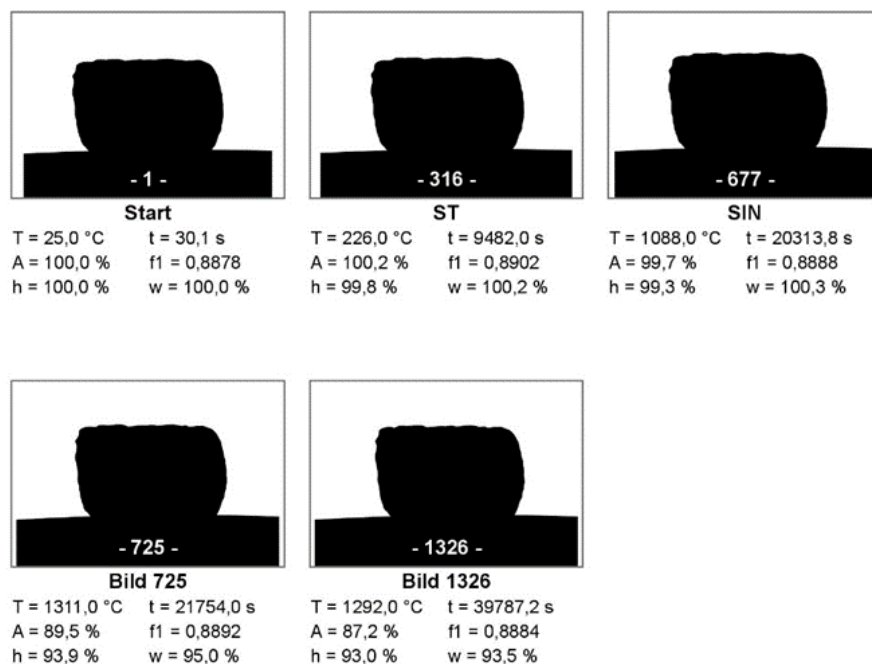

Figure 3.2 *Example of image sequence of images captured by the machine at different temperature during a heating test on a porcelain sample.*

Figure 3.3. *Hot stage microscopy - Hesse-Instruments, Osterode am Harz.*

3.1.4 Sintering tests and volumetric shrinkage evaluation

Different heating treatments, at temperatures between 1000°C and 1350°C were carried out to evaluate the shrinkage effects on LSD samples. The heating rate was 5 °C/min until 600 °C and 2 °C/min between 600 °C and 1000 °C and 5 °C/min again until reaching the maximum temperature. The details of the heating treatments are shown in table 3.1.

For all the samples the volumetric shrinkage (ΔV) has been calculated with the following formula:

$$\Delta V\% = \frac{V1 - V2}{V1} \qquad .$$
(3.1)

Where *V1* and *V2* are the volume of the green and sintered samples respectively measured by manual calliper. The measurements of each dimension were repeated three times for each sample to reduce the casual error.

After the heating treatments, the samples were used for density and porosity measurements, as explained in the following paragraph.

Table 3.1: *Heat treatments for the porcelain samples.*

Treatments	T(°C)	Heating rate (600 °C)	Heating rate (1000°C)	Dwell time (hours)
1	1000	2 °C/min	5 °C/min	1
2	1000	2 °C/min	5 °C/min	3
3	1000	2 °C/min	5 °C/min	5
4	1100	2 °C/min	5 °C/min	1
5	1100	2 °C/min	5 °C/min	3
6	1100	2 °C/min	5 °C/min	5
7	1200	2 °C/min	5 °C/min	1
8	1200	2 °C/min	5 °C/min	3
9	1200	2 °C/min	5 °C/min	5
10	1250	2 °C/min	5 °C/min	1
11	1250	2 °C/min	5 °C/min	3
12	1250	2 °C/min	5 °C/min	5
13	1300	2 °C/min	5 °C/min	1
14	1300	2 °C/min	5 °C/min	3
15	1300	2 °C/min	5 °C/min	5
16	1350	2 °C/min	5 °C/min	1
17	1350	2 °C/min	5 °C/min	3
18	1350	2 °C/min	5 °C/min	5

3.1.5 Density and porosity measurements

3.1.5.1 Pycnometer analysis

A sample of porcelain powder obtained by the drying of the slurry was used to measure the real density by pycnometer analysis. The device used is a gas pycnometer (Gas Pycnometrie, POROTEC, Germany) and Helium is the gas adopted to determine the volume of the sample as it can penetrate among the smallest grains permitting to approach the real volume.

During the test, a sample chamber (Vsc) of known volume is pressurized to a target pressure with the Helium gas, then this pressure is recorded (P_1). At this point a valve is opened and the gas can spread into a second reference chamber, which is a chamber of known volume (V_f). When the balance is reached, the system measures the pressure again (P_2) and calculates the volume on the basis of the volumes of the two chambers and the pressures measured. By knowing the real volume and the weight of the sample, the real density can be calculated directly.

The real volume (V_{SAMPLE}) is then calculated as:

$$V_{SAMPLE} = Vsc - (\frac{Vf}{\frac{P1}{P2}} - 1) \ , \tag{3.2}$$

Where V_{SC} is the volume of the sample chamber, Vf is the volume of the expansion chamber while P_1 and P_2 are the pressure inside the sample chamber and the final pressure.

3.1.5.2. Archimede's method

The density of the sintered sample and the value of closed and open porosity have been calculated by Archimede's method according to ISO 18754[34].
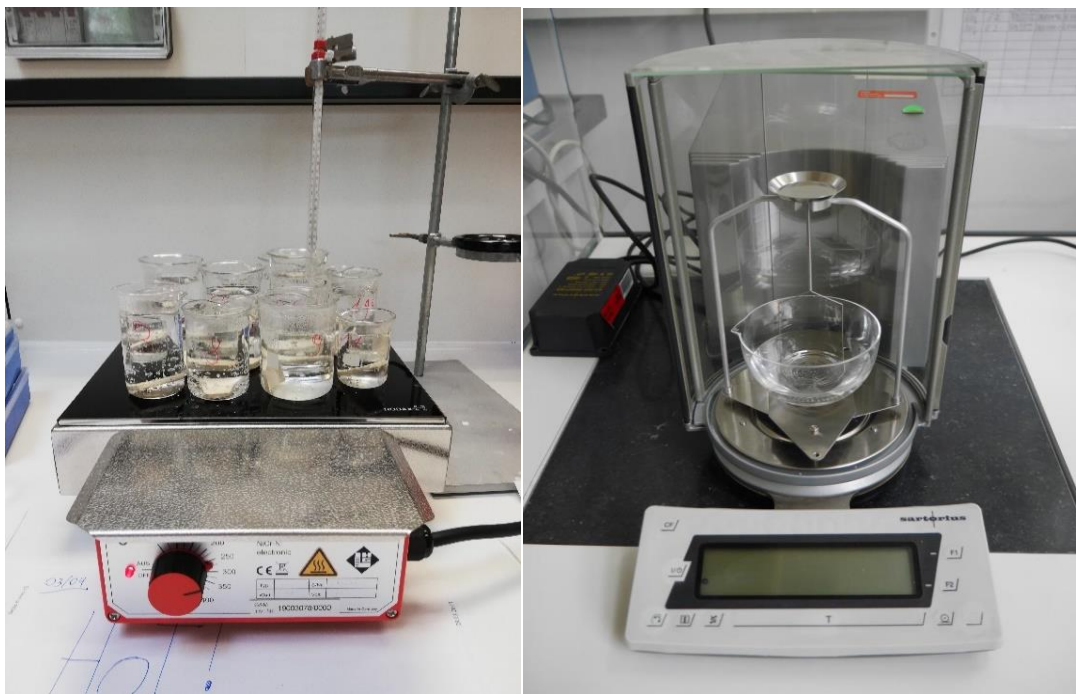

Figure 3.4. *On the left: boiling submerged samples. On the right: Precision balance and Archimede's apparatus from Sartorius.*

The method started with the measurement of the dry mass (M_d) of each sintered sample by a high precision balance (Sartorius, Germany). Subsequently, the samples were immersed in bequers filled with pure water at boiling point, then boiled for two hours. Then the samples were dried superficially with a wet paper to remove only the excess water on the surface and their wet mass (M_w) was measured. Finally, the immersed mass (M_i) was calculated by submerging the samples one by one in an underwater balance support, the Archimede's apparatus and the support are shown in figure 3.4.

In order to reduce systematic errors, both wet and immersed mass were measured three times and their average was chosen for the calculation. With these data and the following formula was possible to calculate the volume of open porosity (V_{OP}), of the sample (V) and its apparent (ρa) and bulk density (ρb). The density of the water (ρw) used must be known, in this case was adopted the density of distilled water at 25°C.

$$Vop = (Mw - Md)/\rho w \tag{3.3}$$

$$V = (Mw - Mi)/\rho w \tag{3.4}$$

$$\rho a = \left(\frac{Md}{Md - Mi}\right) \cdot \rho w \tag{3.5}$$

$$\rho b = \left(\frac{Md}{Mw - Mi}\right) \cdot \rho w \tag{3.6}$$

ρ_a corresponds to the ratio of the dry mass to its apparent solid volume, ρ_b corresponds to the ratio of the mass of the dry material to its bulk volume.

Then, the percentage of open porosity (OP) has been calculated as shown below:

$$OP = Vop/V \tag{3.7}$$

Knowing the density of the material (ρm), from the previous pycnometer analysis, it was possible to calculate the percentage of total porosity (TP) and consequently the closed porosity CP.

$$TP = 1 - (\rho b/\rho m) \tag{3.8}$$

$$CP = TP - OP \tag{3.9}$$

3.1.6 X-ray diffraction

In order to know the correct phase composition of the porcelain, XRD analyses of green and sintered samples were performed by means of D8 Advance (Bruker, Massachusetts, USA). The green part was dried to obtain the sample, while a sintered sample, treated at 1300 °C for an hour, was ground to obtain a powder sample.

The analysis of an X-ray diffraction spectrum (XRD), while not providing direct information on the chemical composition of a sample, allows to define and quantify the crystalline phases present in any material in the first 20 microns of surface. Each crystalline solid has its unique characteristic X-ray pattern which may be used as a "fingerprint" for its identification.

At the base of this technique is the interaction between the incident wave, X-rays, and the crystalline lattice according to Bragg's law: $2\lambda = 2dSin\theta$. This law relates the wavelength of

electromagnetic radiation (λ) with the angle of diffraction (θ) and the lattice spacing in a crystalline sample (d). These diffracted X-rays are then detected and processed. The diffraction peaks obtained from the analysis were then matched to their respective materials by a software.

3.2   PPG-Graphite based ink

For the purpose of the project it was necessary to develop a sacrificial graphite-based ink, as it can be easily eliminated by a heat treatment at a lower temperature than the sintering of the ceramic material. After preparation, the ink was studied by DSC and TG analyses, rheological tests and density measurements.

3.2.1 Ink preparation

Since this ink was intended to be removed, it had to be quick and easy to prepare, preferably made of inexpensive materials. It also needed to have some typical characteristics of robocasting ink, such as the pseudoplastic behaviour and the ability to flow through fine deposition nozzles at modest shear rate without clogging. Since only one layer of ink was to be deposited on the porcelain substrate, the ink has not been designed to have such a high capacity to retain its shape under the load of overlaying layers, which is in general required for robocasting inks.

Furthermore, this ink had to be chemically compatible with the porcelain green part and easily eliminable by subsequent heat treatments, without leaving any by-products or residues after decomposition. Another important feature was the ability to dry quickly to be used in the designed process.

A carbon ink has been already used as a sacrificial ink for robocasting in the building of support structures for complex parts, as described in the work of Martínez-Vázquez F. et al[32]. For this project a graphite-based ink has been adopted. Since water and methylcellulose graphite-based inks resulted in solvent separation, a Polypropylene glycol (PPG)-graphite based ink was found to be more suitable for the process.

The ink was produced mixing a solution of poly-propylene glycol 2000 (Fluka Chemika, Swizerland) with crystalline graphite powder 41%wt (Alfa Aesar – Johnson Matthey Company, USA) by rotary mill (Pulverisette, Fritsch GmbH, Germany) without milling ball, at 400 rpm for 20 minutes. The viscosity of the ink was adequate to be extruded, it was homogeneous and was not absorbed too quickly by the porcelain substrate.

3.2.2 DSC and TG analyses

Differential scanning calorimetry (DSC) and Thermogravimetric (TG) analyses were carried by means of thermal analysis instrument (Mettler Toledo STARe Excellence, USA) to study the degradation process but also the mass change of the ink during heating at a constant rate. It was thus possible to optimise the firing conditions for ink removal.

Figure 3.5. *DSC/TG machine by Mettler Toledo.*

DSC analysis provides data on endothermic and exothermic processes that occur during the processes of heating or cooling of materials by measuring the amount of energy absorbed or released by the sample. This is possible by continuously monitoring the difference in heat flow between a reference material and a test material when heated or cooled at controlled speed.

Differential Scanning Calorimetry is usually used as a rapid test method for determining several material behaviours, such as melting temperature, heat of fusion, glass transition temperature, crystalline phase transition temperature and energy, oxidation induction times, and specific heat or heat capacity.

TGA was also used to measure mass change in the ink sample and investigate the causes related to it, such as decomposition, evaporation or oxidation, in order to optimise the ink removal condition.

3.2.3 Rheological analysis of the ink

Rheology is the study of flow and deformation of materials under applied forces, applicable to all types of materials, fluids, semi-solids such as gels and paste, but also to solid systems such as polymers and composites. It provides information about the mechanical response to a dynamics stress or strain.

Rheological properties can be measured by means of rotational or by capillary rheometer. Usually two classes of measurements are run with the rheometer: viscosity measurements, for an evaluation of the flow properties, and oscillatory measurements. Rheological properties are crucial for a robocasting ink and they have been examined by rotational test. A stress-controlled rotational rheometer (MCR 301, Anton Paar GmbH, Germany) was used to perform viscosity measurement on PPG-Graphite ink (Figure 3.6).
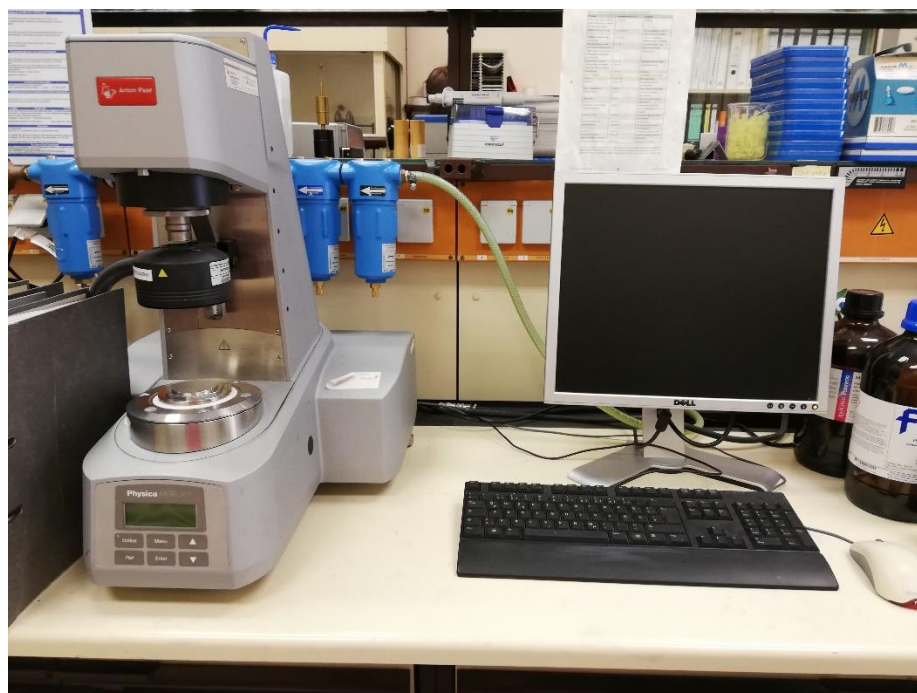

Figure 3.6. *Rheometer used during the ink test.*

Viscosity is the measure of resistance to deformation by shear stress or tensile strength, also defined as the resistance of the fluid to flow. By applying a tangential force (F) to the area (A) of the fluid, as in Figure 3.7., a shear stress is generated. Assuming that the fluid is divided into parallel layers that flow tangentially over each other between two area plans (A) and distant

(*D*), the application of such shear stress causes the fluid to flow through the direction set with a speed decreasing from the upper to the lower layers. The viscosity *(η) = [Pa · s]* and other rheological parameters can be written as in following formulas:

$$\eta = \frac{\tau}{\dot{\gamma}} \rightarrow \tau = \eta \cdot \dot{\gamma}, \tag{3.10}$$

$$\tau = \frac{F}{A}, \tag{3.11}$$

$$\gamma = \frac{S}{D}, \tag{3.12}$$

$$\dot{\gamma} = \frac{d\gamma}{dt}. \tag{3.13}$$

Where τ is the shear stress [Pa], γ the shear deformation while the rate at which fluid layers move past each other is the shear rate $\dot{\gamma} = [s^{-1}]$.
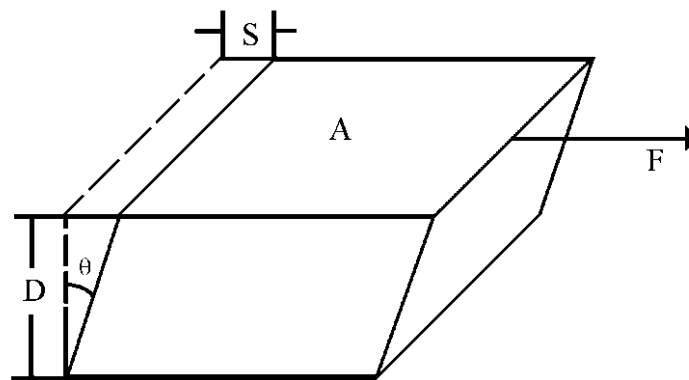

Figure 3.7. Generation of shear stress and fluid viscosity.

For Newtonian fluids, viscosity is not dependent on shear rate or stress and the relation between shear stress and shear rate is linear (3.10). Whereas, for pseudoplastic or dilatant fluid the viscosity depends on the shear rate and it is called apparent viscosity, it can be written as in (3.14) and its value is obtained from steady shear measurement.

$$\eta_a = K\dot{\gamma}^n \tag{3.14}$$

Where *n* is the fluid flow index, and is *0<n>1* for pseudoplastic fluid (shear thinning fluid) or *n>1* for dilatant (shear thickening fluid). An increasing shear rate reduces apparent viscosity of pseudoplastic fluids and it's called shear thinning behaviour, as shown in Figure 3.8. Thus, $\dot{\gamma}$ is an important parameter to consider to analyse the behaviour of a pseudoplastic fluid as might be an ink to be extruded.
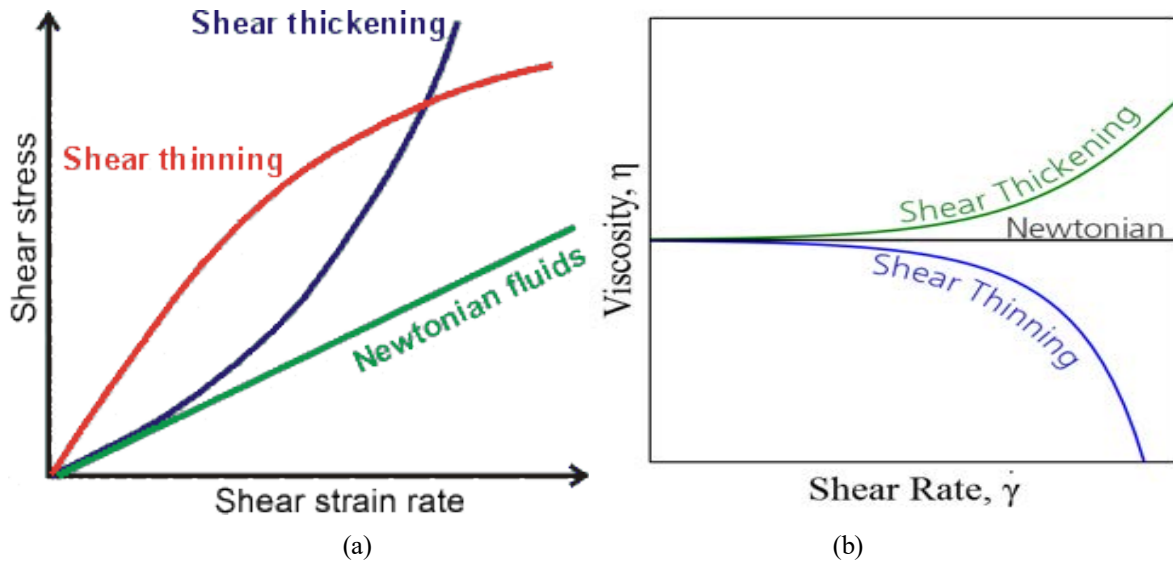
Figure 3.8. *Shear stress as a function of shear rate for different kind of fluid (a), and shear thinning fluid (pseudoplastic fluid) and shear thickening fluids (dilatant fluid) as a function of shear rate (b).*

Analytical solutions for complex nozzles are rather difficult to achieve because of the shear and time dependence of the viscosity. But, the shear rate and other rheological parameters can be estimated using analytical solutions for isothermal, steady flow of Newtonian and Power-law fluids through a circular tube. The power law model is an ideal model for shear thinning fluids and for a power-law fluid the viscosity is:

$$\eta(\dot{\gamma}) = K\dot{\gamma}^{n-1} , \qquad (3.15)$$

where *K* is the consistency coefficient and *n* is, in this case, the power law index.

With the extruder's nozzle approximating to a circular tube of radius R, the shear rate in the nozzle is maximum at the wall and decrease toward the center of the tube until becoming zero (Figure 3.9). Knowing the volumetric flow rate *(Q)=[cm³/s]* and the radius (R) of the nozzle is possible to calculate the apparent shear rate at the wall that for a Newtonian fluid is:

$$\dot{\gamma}_a = \frac{4Q}{\pi R^3} , \qquad (3.16)$$

while for a Power-law fluid the true shear rate at the wall will be:

$$\dot{\gamma}_w = \frac{4Q}{4\pi R^3} \cdot \left(3 + \frac{1}{n}\right) = \frac{\dot{\gamma}_a}{4} \cdot \left(3 + \frac{1}{n}\right), \qquad (3.17)$$

$$\dot{\gamma}_r = \frac{V_0}{R} \cdot \left(\frac{n+1}{n}\right) \cdot (r/R)^{1/n} \,, \tag{3.18}$$
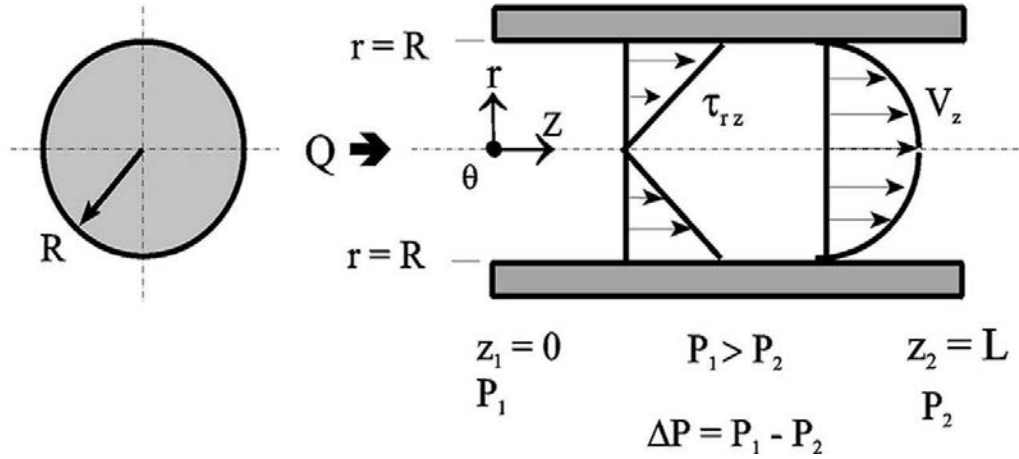
where V_0 is the maximum velocity at center of the tube.

Figure 3.9. *Isothermal flow through circular tube of radius R.*

The apparent viscosity (η_a) of the ink was measured as a function of increasing shear rate (from $\dot{\gamma} = 0.01\text{-}150 \ s^{-1}$ at 40 value points with logarithmic spacing) by rotational rheometer test using a cone-plate geometry. An equilibration time of 5 s was observed at each value of shear rate prior to reading the shear stress.

The ink's flow properties can be approximated by the Herschel-Bulkley model, this model describes non-Newtonian behaviour after yielding and is basically a power law model with a yield stress term. The rheometer software compares the measured shear stress value with those obtained by means of a three-parameter rheological model Herschel-Bulkley fluid, shown in the following equation:

$$\tau = \tau_0 + k(\dot{\gamma})^n \tag{3.19}$$

Three parameters characterize this relationship: the consistency factor k, the shear thinning index n, and the yield shear stress τ_0. The yield stress is a property associated with numerous types of complex fluids, whereby the material does not flow unless the applied stress exceeds a certain value.

3.3   Process and equipment

As explained above, the process developed is based on the hybridization of AM techniques, specifically Layer-wise slurry deposition (LSD) and Robocasting/DIW for the fabrication of porcelain ceramic with built-in microchannels. The process can be divided in different stages described in the following paragraphs. The equipment used was a custom setup, as shown in the Figure 3.10.

3.3.1 First layer-wise deposition of porcelain slurry

The first step involved the deposition of the porcelain slurry performed through the LSD technique, until the desired number of layers were obtained. The machine used for the deposition was a miniaturization of an LSD machine, developed by BAM (Figure 21). It was composed of a mobile shaft which provides the deposition of the slurry on a platform heated to about 120 °C. With each movement of the shaft along the Y-axis, the platform lowers along the Z-axis by a certain thickness, that will be the thickness of the deposited layers.

The movement of the platform and the shaft is controlled by computer, from which it is possible to modify the motion parameters of the machine. The temperature of the platform speeds up the drying of the layers and thus the process.
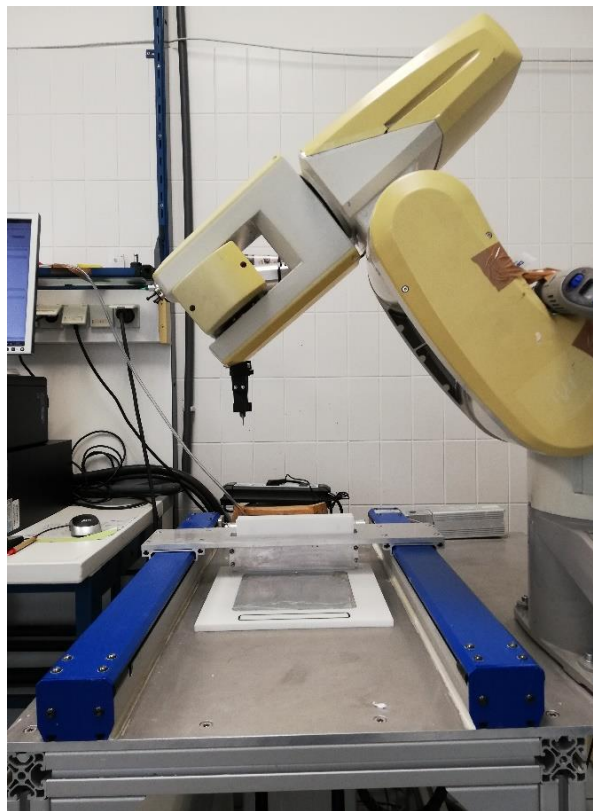

Figure 3.10. *Machine set up used during the process, Mini-LSD machine and Robot arm.*

The first layer of porcelain slurry was deposited on an aluminium foil, glued on a porous metal platform, by means of a doctor blade. The aluminium foil was necessary to remove easier the part after the process. As explained above, the substrate for the deposition of the successive layers is formed by the previous layer which act as a porous mould. The deposition was performed via a Teflon doctor blade prototype, which also works as slurry reservoir.

The porcelain slurry is a stable suspension, but it was necessary to stir it by means of a mixer before the deposition to avoid the presence of agglomerates, which can cause defect during the process. Moreover, the viscosity of the porcelain slurry should not be too high since the layers were deposited by gravity.

3.3.2 Drilling process

The second step was the drilling process in order to dig the channel to be filled with ink. The drilling was carried out by means of a mini drill (Dremel 225-flex-shaft attachment, Germany) installed on a robot arm (Mitsubishi RV-E4NM, Japan). By programming the movement of the robot arm, it was possible to drill into the dried porcelain layers according to a precise path. The size of the channels was defined by the drill tip, a tip with a diameter of 0.9 mm was used.

3.3.3 Graphite-based Ink printing – Robocasting

The next step was to deposit the ink inside the prepared channel in order to fill it up (Figure 3.11). The printing of the ink was made by means of an extruder (Vipro-HEAD3 – ViscoTec Pumpen- u. Dosiertechnik GmbH, Germany). The ink, placed inside a syringe, after removing any trapped bubbles was compressed into the extruder that deposited it in the channel through a cylindrical nozzle (Precision Tip, Nordson EFD, USA) with a diameter of 0.84 mm.

Figure 3.11. *Example of a simple drilling and ink printing path.*

This tool was also installed on the robot arm, in correspondence of the "hand" of the robot (Figure 3.12). By turning the hand, the robot changed tool and allowed to follow the path previously dug. The extruder operates through a stepper motor, controlled by a control unit (C5-motor controller, Nanotec - plug e drive, Germany). Its working speed can be modified and adapted to the process.

Volumetric flow rate tests have been carried out on the extruder. The tests consisted of extruding ink into a vessel at different rpm of the motor for one minute and then measuring the mass of the extruded material. Knowing the density of the ink components, it was possible to estimate the volume of extruded material over time.

Further tests have been run to evaluate the influence of the robot and extruder parameters on the process. Drilling test at different speeds of the robot and drill were performed to evaluate the shape and size of the channels, in addition visual test has been run to evaluate the size of the extruded filament on a porcelain substrate in relation to the working speed of the extruder in order to adapt the dimension of the extruded filament with that of the channel drilled. The width of the filament was estimated using image analysis software (ImageJ software, USA).

Figure 3.12. *Tools installed on the robot arm during an experiment.*

3.3.4 Second Layer-wise slurry deposition

A second slurry deposition has been made to cover the built channel and obtain a green part with an ink filament housed inside the channel embedded within the green part.

3.3.5 Firing of the green parts

Thanks to the results obtained from the thermal analysis of slurry and ink, it was possible to define and optimize the type of heat treatment to be performed. First, the parts were let drying in air for one day and then heat treated at 700 °C, by means of a sintering oven (Carbolite, UK), to achieve complete elimination of the graphite-based ink inside the channel. The heat rate was 2°C/min, and the dwell time at 700 °C was 1 hour.

The following heat treatment was the sintering of the parts at a temperature of 1300 °C, dwell time one hour. The heat rate was 5°C/min until 600 °C, then 2°C/min up to 1000 °C and 5°C/min until reaching the target temperature. At the end of the process, finished ceramic parts with incorporated channels were obtained.

3.4 Microchannel investigation

Optical and digital microscopic observations (VHX digital microscope, Keyence) and furthermore analysis by X-ray computed tomography (µCT 40, Scanco Medical, Switzerland) have been performed to investigate the microchannel structure inside the finished parts.

Computed X-ray tomography (CT) is a non-destructive technique for displaying internal elements within solid objects and for obtaining information about their 3D geometries. Micro computed tomography or "microCT" is 3D X-ray imaging in a small scale with a greatly increased resolution.

It consists of a micro-focus X-ray source that illuminates the object and a series of X-ray detectors collect enlarged projection images. A computed tomography image is typically called a slice, i.e. virtual cross sections that cut the object. Based on hundreds of angular views acquired as the object rotates, a computer develop a series of these slices and It is then possible to move between the cross sections to inspect the internal structure of the object.

Figure 3.13. *Micro computed tomography machine by Scanco Medical used for the analysis.*

Chapter 4: Results and discussions

4.1 Porcelain Slurry characterization

4.1.1 Particle size distribution

The result of the particle size analysis is a volume weighted particle size distribution. The particle size distribution and the cumulative plot are shown in the Figure 4.1.
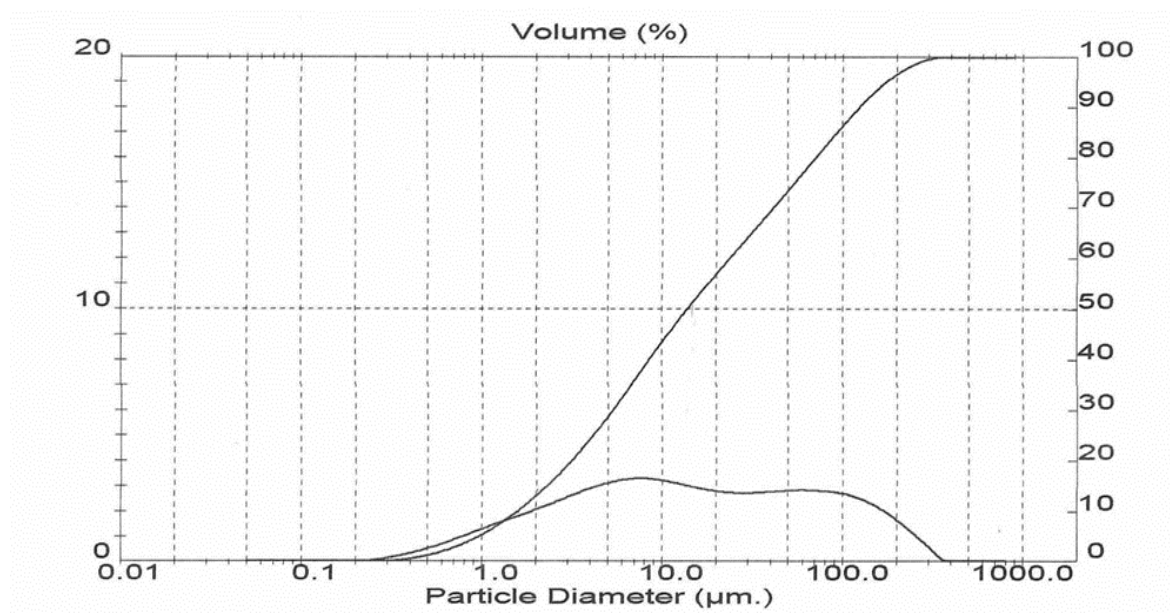

Figure 4.1. *Volumetric particle size distribution and cumulative plot.*

From the graph a large distribution with a significant proportion of oversized particles can be noticed. The median particle size by volume [D (v, 0.5)], indicating the maximum diameter possessed by 50% of the measured powder, is 13.84 µm. 90% of the measured powder has a diameter of maximum 125.70 µm. Generally, a dimensional range between 100 nm and 100 µm is suitable for the LSD process as described in chapter two. Other percentiles and result statistics are reported in the table below.

Table 4.1: *Particle size analysis results*

Mean Diameters Parameters	Size (μm)
D (v, 0.1)	1.58
D (v, 0.5)	13.84
D (v, 0.9)	125.70
D (v, 0.97)	209.75
D [4, 3]	41.62
D [3, 2]	4.30

4.1.2 DTA and TGA results

In order to investigate weight change characteristics and thermal phenomena that occur during porcelain firing, TG analysis were performed. The TG measurement results are shown in the following figure.
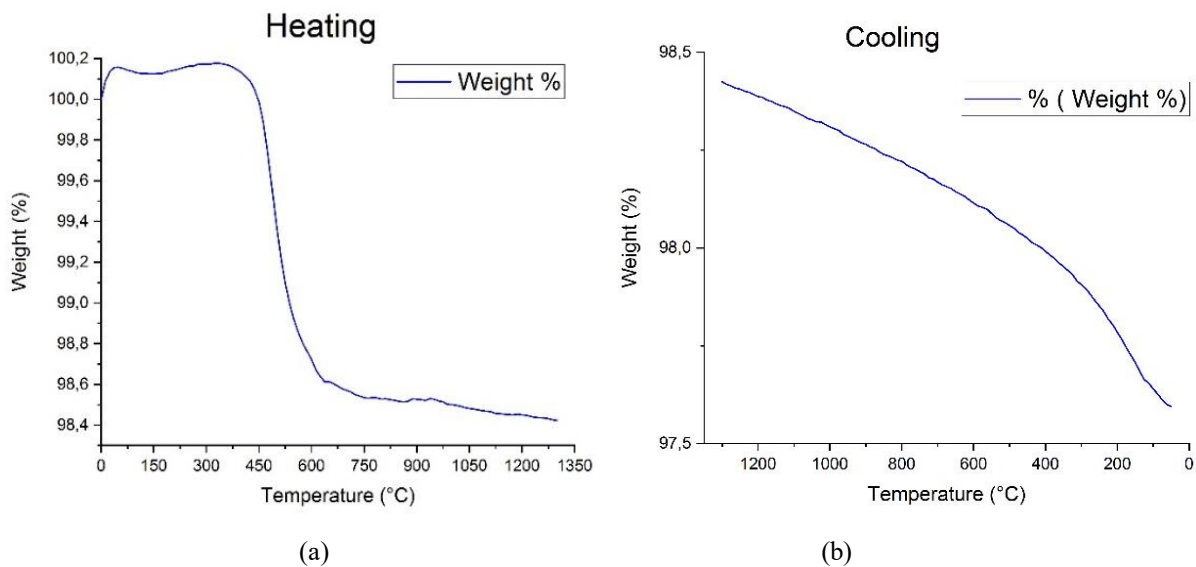

(a)   (b)

Figure 4.2. *TG measurements results for porcelain. Heating to 1300°C (5°C/min) (a) and cooling (b)*

No weight loss is detected by heating up to 400°C, which indicates the absence of adsorbed water after the drying step. An appreciable weight loss occurs between 400°C and 800°C. Further weight loss is observed during cooling. A total weight loss of 1.5% is observed upon

heating, likely caused by dehydroxylation of kaolinite to form metakaolinite according to the following reaction:

$$Al_2Si_2O_5(OH)_4 \rightarrow Al_2Si_2O_7 + 2H_2O$$
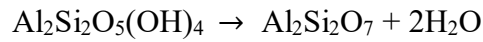
4.1.3 Optimization of the firing condition

Figure 4.3. shows densification curves obtained by hot stage microscopy at temperatures between 1000 and 1300 °C with same heating rate of 10°C/min. The curves show an onset of sintering and densification around 1080°C for all the sample, proving that heat treatment at lower temperatures would not result in adequate densification of the samples.

Figure 4.4 displays the test for the sample treated at 1300 °C, a sintering and densification onset is noted at temperatures of ca. 1085°C.
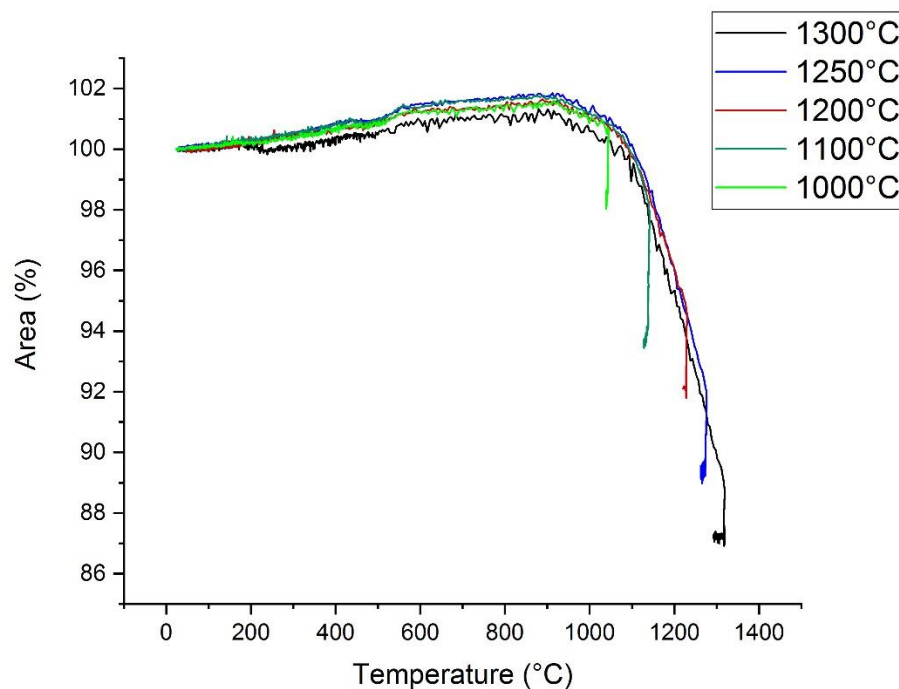

Figura 4.3. *Densification curves at temperature between 1000°C and 1300°C by HSM. The heat rate was 2°C/min up to 500°C and 10°C/min until reaching the maximum temperature, the target temperature was kept for 5 hours.*

Isothermal densification curves at temperatures between 1000°C to 1300°C, dwell time of 5 hours are shown in figure 4.5. It is possible to observe how a heat treatment at a temperature of 1000 °C would have a negligible effect on the densification of the sample, while the area shrinkage increases with the temperature (ca. 14% at 1300°C).
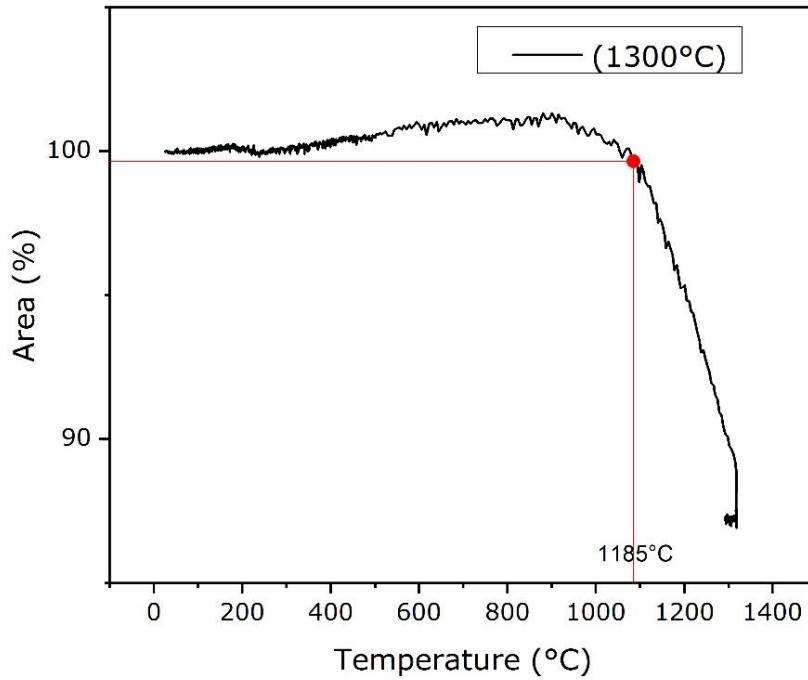
51

Figura 4.4. *Densification curve for heat treatment at temperature of 1300°C, dwell time 5 h.*

Another important observation is that the densification did not increase significantly with the heat treatment time:in fact, for each temperature it reached a plateau value after about 100 min. Firing at 1300°C allows maximum densification to be achieved already after 60 minutes of treatment.
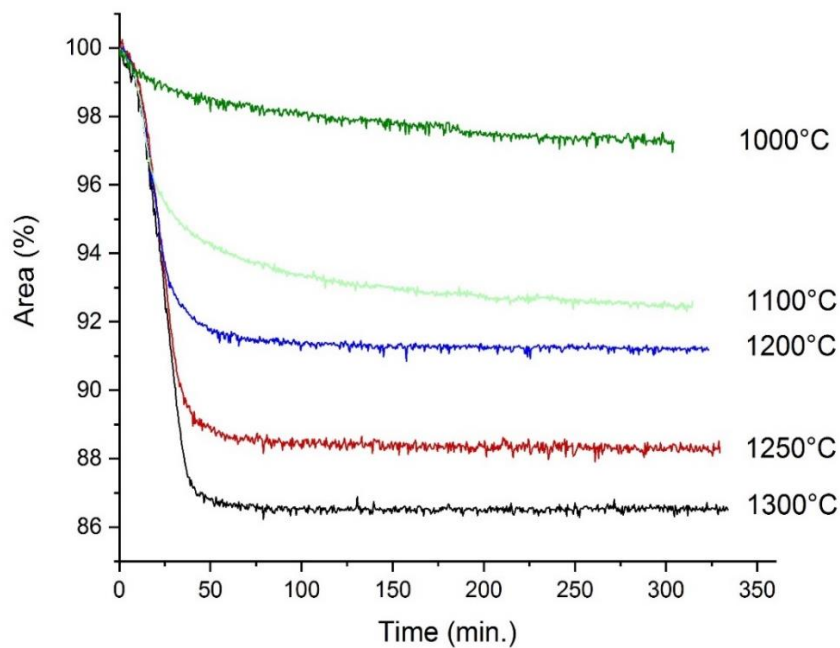

Fig.4.5. *Isothermal densification curves at temperatures between 1000°C and 1300°C.*

Linear and volumetric shrinkage were also estimated. The results listed in table 4.2 show a maximum volumetric shrinkage of 16,89% ± 0,01 after 1h at 1300°C; high values of shrinkage were also measured at 1250°C and 1350°C.

Table 4.2: *Shrinkage evaluation of the samples sintered at temperature between 1000 and 1350 °C, dwell time of 1 h.*

Sintering temperature	Δt%	Δw%	Δl%	ΔV%
1000 °C	2,15% ± 0,03	0,52% ± 0,01	0,93% ± 0,01	3,55% ± 0,05
1100 °C	1,56% ± 0,01	2,31% ± 0,01	1,81% ± 0,01	5,57% ± 0,01
1200 °C	1,94% ± 0,01	3,16% ± 0,01	4,25% ± 0,01	9,08% ± 0,01
1250 °C	6,71% ± 0,02	3,26% ± 0,02	4,99% ± 0,01	14,20% ± 0,03
1300 °C	6,67% ± 0,01	5,67% ± 0,01	5,59% ± 0,01	16,89% ± 0,01
1350 °C	4,97% ± 0,01	5,16% ± 0,01	5,47% ± 0,01	14,8% ± 0,01

In samples treated above 1300 °C, a smooth, translucent phase was noted. This may be due to the presence of feldspars. The Feldspars are natural silicates ($SiO4$-based minerals) which, when fired, vetrify to form high viscosity glassy phase. The liquid phase, after the cooling, solidifies to form a glassy matrix that gives the product its translucid appearance (Figure 4.6.).
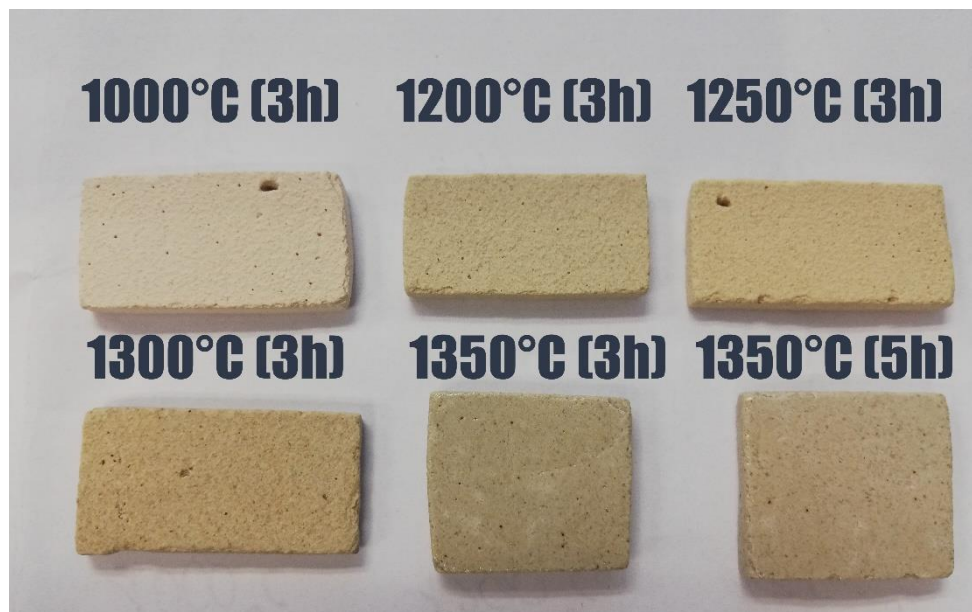

Fig.4.6. *Image of some LSD porcelain samples sintered at increasing temperatures, a change in colour and surface was noted for the different treatment temperatures.*

4.1.4 Density and porosity measurements

The results of the pycnometer analysis are reported in table 4.3. The technique allows to measure the material real density, in contrast with the Archimedes method in which is not possible to avoid taking into account the closed porosity.

Table 4.3: *Real density of porcelain measured with pycnometer before sintering.*

Porcelain powder	
Average sample volume	1.202 cm^3 ± 0.001
Real density	2.690 g/cm^3 ± 0.001

Table 4.4: *Volume of open porosity, bulk volume, apparent solid and bulk density for all the treatments. Highlighted are the values for the best heat treatments.*

Sintering temperature and time	$\rho_{apparent}$ (g/cm^3)	ρ_{bulk} (g/cm^3)
1000 °C – 1h	2,445 ± 0,005	1,795 ± 0,007
1000 °C – 3h	2,462 ± 0,004	1,790 ± 0,018
1000 °C – 5h	2,483 ± 0,009	1,813 ± 0,017
1100 °C – 1h	2,394 ± 0,004	1,882 ± 0,007
1100 °C – 3h	2,385 ± 0,005	1,859 ± 0,006
1100 °C – 5h	2,399 ± 0,023	1,884 ± 0,021
1200 °C – 1h	2,336 ± 0,002	2,057 ± 0,013
1200 °C – 3h	2,291 ± 0,006	2,002 ± 0,015
1200 °C – 5h	2,270 ± 0,015	1,970 ± 0,032
1250 °C – 1h	2,280 ± 0,012	2,062 ± 0,024
1250 °C – 3h	2,268 ± 0,011	2,066 ± 0,034
1250 °C – 5h	2,353 ± 0,030	2,070 ± 0,039
1300 °C – 1h	2,277 ± 0,017	2,134 ± 0,028
1300 °C – 3h	2,257 ± 0,011	2,139 ± 0,028
1300 °C – 5h	2,196 ± 0,0014	2,034 ± 0,048
1350 °C – 1h	2,214 ± 0,003	2,116 ± 0,006
1350 °C – 3h	2,178 ± 0,002	2,083 ± 0,014
1350 °C – 5h	2,161 ±0,002	2,035 ± 0,010

Density measurements with Archimedes method was performed for LSD samples heat treated at same condition as hot stage microscopy test. Table 4.4 shows the results of this analysis. A water density (ρ_w) value of 0.997 g/cm³ at 24,5°C was used for the calculations.

Comparing the real density value with the previous measured density values reported in table above, it can be seen that the measurement with the helium pycnometer gives a higher result, as the He atoms can penetrate in the porosity of the powdered sample.

Moreover, table 4.4. highlights how the bulk density is always smaller than the apparent solid density, according to the fact that the bulk volume is the sum of the respective volumes of the solid material, the open pores and the closed pores while the apparent solid volume takes into account only the solid volume and the closed porosity.

Table 4.5: *Apparent, closed and total porosity for all the treatments. Highlighted are the values for the best heat treatments.*

Sintering temperature and time	Open Porosity	Closed Porosity	Total Porosity
1000 °C − 1h	26,61% ± 0,4	6,69% ± 0,13	33,30% ± 0,28
1000 °C − 3h	27,28% ± 1,03	6,20% ± 0,41	33,48% ± 0,66
1000 °C − 5h	26,97% ± 0,96	5,64% ± 0,32	32,61% ± 0,65
1100 °C − 1h	21,39% ± 0,38	8,67% ± 0,18	30,06% ± 0,28
1100 °C − 3h	22,06% ± 0,28	8,87% ± 0,12	30,93% ± 0,22
1100 °C − 5h	21,46% ± 0,85	8,52% ± 0,45	29,97% ± 0,78
1200 °C − 1h	11,94% ± 0,64	11,61% ± 0,17	23,54% ± 0,49
1200 °C − 3h	12,62% ± 0,72	12,98% ± 0,31	25,60% ± 0,56
1200 °C − 5h	13,24% ± 1,54	13,57% ± 0,49	26,81% ± 1,15
1250 °C − 1h	9,54% ± 1,04	13,81% ± 0,46	23,36% ± 0,88
1250 °C − 3h	8,90% ± 1,59	14,31% ± 0,48	23,21% ± 1,25
1250 °C − 5h	12,02% ± 1,52	11,07% ± 0,84	23,09% ± 1,43
1300 °C − 1h	6,25% ± 1,08	14,44% ± 0,59	20,69% ± 1,03
1300 °C − 3h	5,20% ± 1,24	15,30% ± 0,42	20,51% ± 1,04
1300 °C − 5h	7,39% ± 2,31	17,04% ± 0,68	24,42% ± 1,77
1350 °C − 1h	4,46% ± 0,24	16,92% ± 0,11	21,38% ± 0,22
1350 °C − 3h	4,37% ± 0,66	18,23% ± 0,19	22,60% ± 0,52
1350 °C − 5h	5,85% ± 0,47	18,53% ± 0,12	24,38% ± 0,36

The previous tables point out that the sintering process has allowed the reduction of the intergranular spaces and therefore of the porosity with a consequent increase of the bulk density, as also shown in the following figures 4.7 and 4.8.
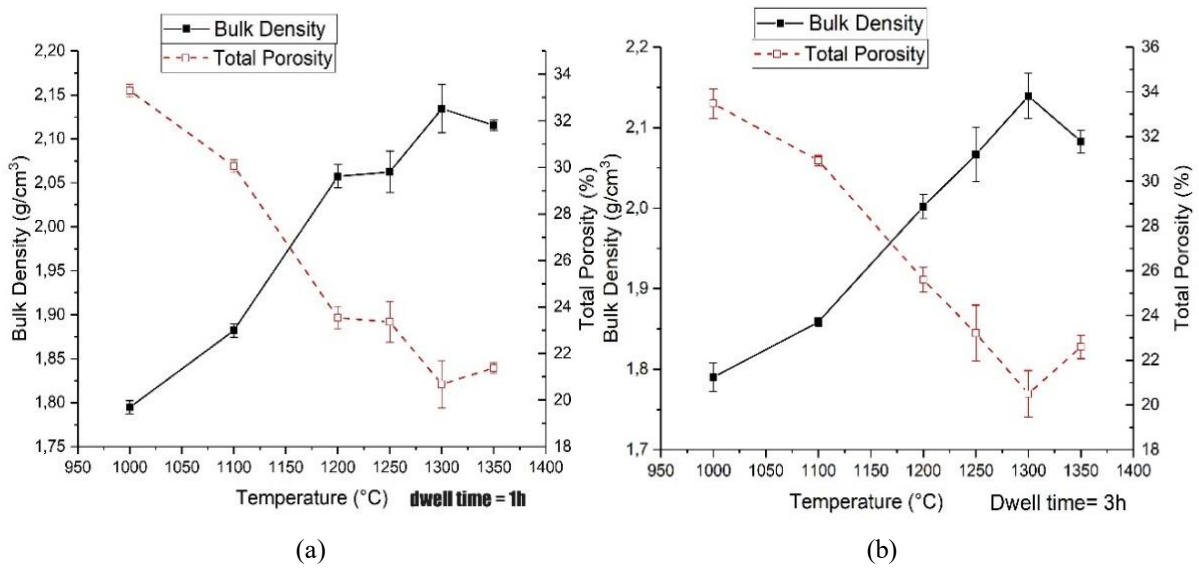
Fig.4.7. *Comparison between bulk density and total porosity trend at different sintering temperatures, for one hour (a) and 3 hours of dwell time (b).*
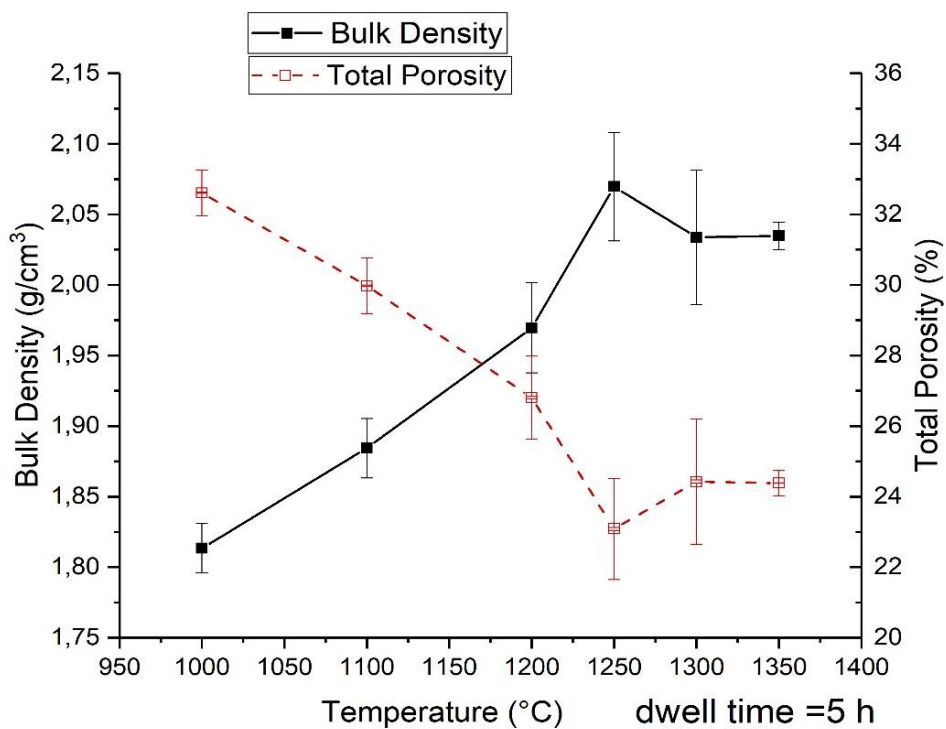

Figure 4.8. *Bulk density and total porosity trend at different temperatures of treatment and same dwell time (5h).*

The heat treatments that allow best densification with minimum porosity value are those that provide heating up to 1300 ° C, in accordance with the HSM test results, dwell time of 1 and 3 hours. Given almost identical values of density and porosity, the best heat treatment is obviously

56

the one that allows to obtain them in the shortest time and with less use of energy clearly, hence, the one that provides a dwell time of one hour.

For the heating treatment at 1350°C, it was possible to notice a slight decrease in density (or at least not an increase in densification) and a consequent increase in total porosity compared to that at 1300°C. This could be due to the expansion of trapped gas in the glass phase formed during the feldspar transformation; this bloating effect was not detected visually, but is well known for porcelain materials[23,35] and can also cause expansion and large pores on the sample.

4.1.5 XRD results

In order to know the phase present in the slurry used, x-ray diffraction analyses were carried out on samples of material, before and after sintering. The results are shown in the following images and the phase quantification is reported in table 4.6.
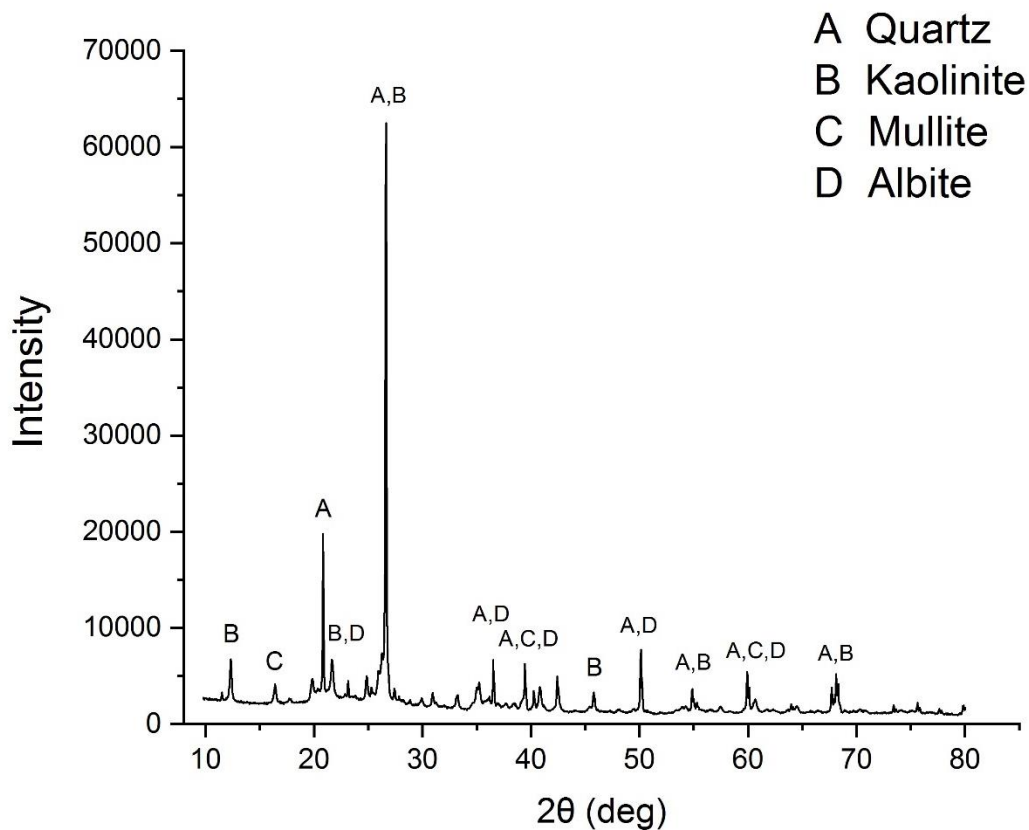

Figure 4.9. *XRD pattern for porcelain slurry.*

The main phases that comprise the slurry were; Quartz (50,37%), Mullite (19,89%), Kaolinite (17,18%) and Albite (12,55%). The high percentage of quartz (SiO_2) and the presence of mullite [$Al_6O_5(SiO_4)_2$] are typical in commercial clays. Kaolinite [$Al_2Si_2O_5(OH)_4$] is a clay mineral always present in porcelain while Albite ($NaAlSi_3O_8$) is a mineral of the feldspar group.

After sintering at 1300°C the high temperature crystalline phases were quartz and mullite, and the phase composition of the LSD samples changed in a similar way to the traditional porcelain slip-casted, with an increase in the amount of mullite (table 4.6). Kaolinite is first transformed into spinel and then completely into mullite.
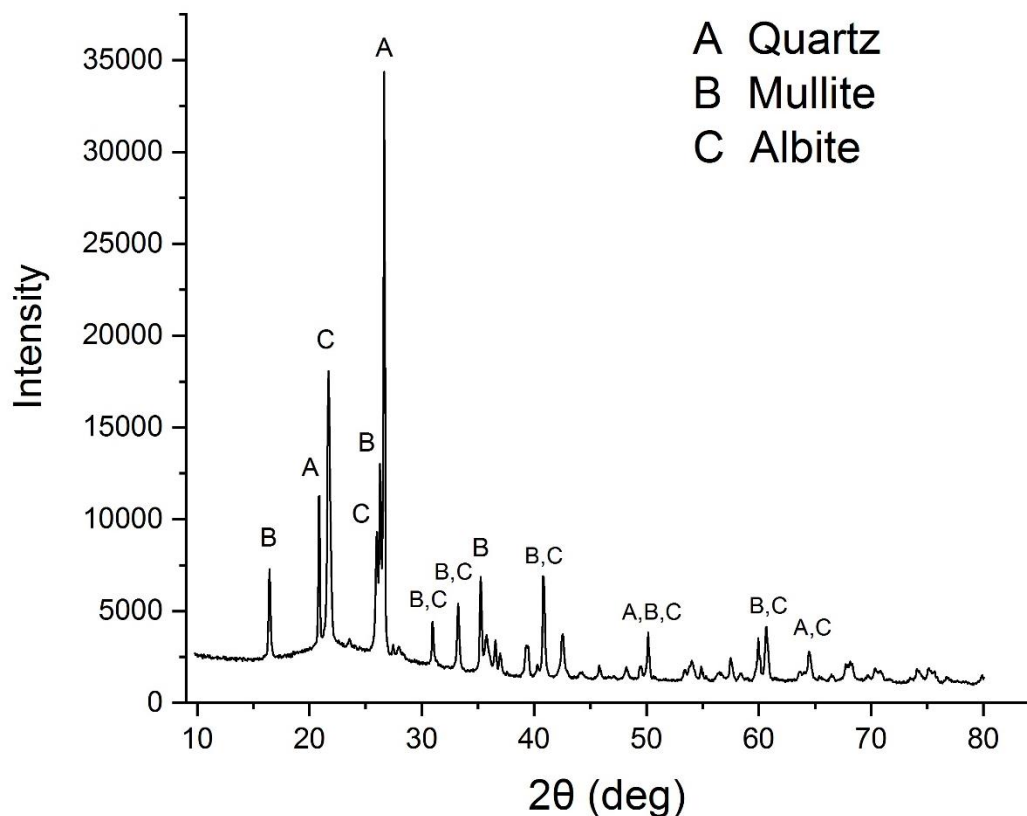

Figure 4.10. *XRD pattern for porcelain sintered at 1300°C/1h.*

Table 4.6: *Phase composition of porcelain slurry and sintered samples.*

Phase (wt%)	Slurry	Sintered at 1300°C
Quartz	50,37 %	29,5 %
Mullite	19,89 %	47,96 %
Kaolinite	17,18 %	-
Albite	12,55 %	22,54 %

4.2 PPG- Graphite based ink characterization

4.2.1 DSC and TG analyses results

Differential scanning calorimetry and thermogravimetric analysis were performed on the ink in order to optimise the firing condition for the ink removal. The ink sample was heated at a constant heat rate of 5 °C/min up to 1400°C. The results of the analyses are shown in the figure 4.11.

From room temperature to about 150°C the curves do not show any significant change; starting from 180°C to about 250°C, a considerable weight loss of more than 70% was detected in the TG curve, while DSC curve shows a sharp exothermic peak: this is mainly due to the thermal degradation of the PPG 2000.
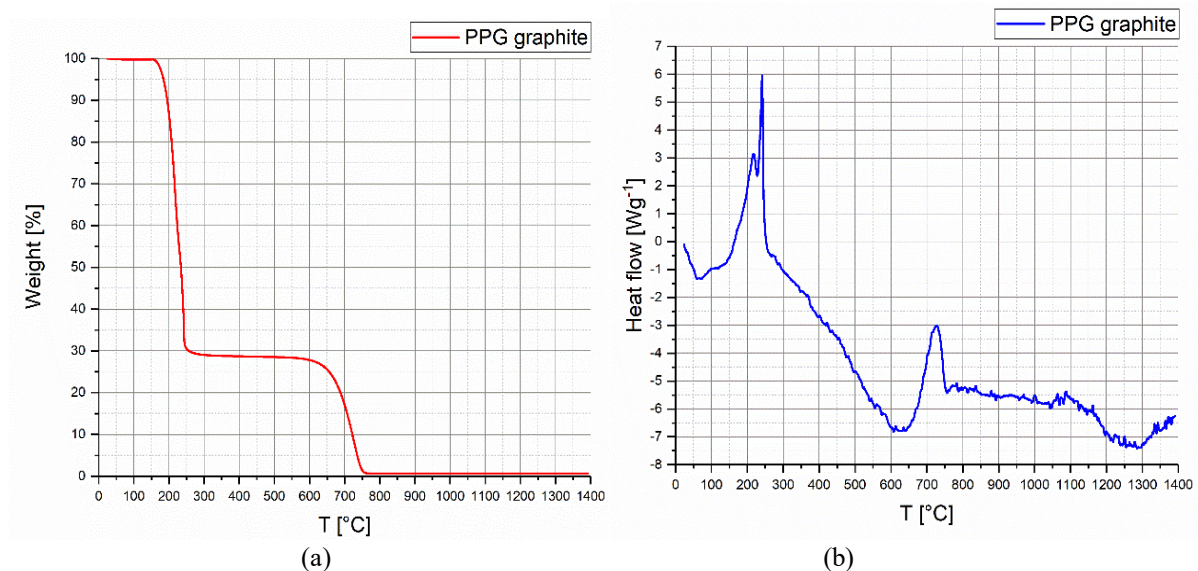

Figure 4.11. *TG (a) and DSC(b) traces for the PPG-Graphite based ink.*

In the range between 300°C and 600°C there is not significant weight change while from 650°C to 750°C TG curve shows a weight loss of about 28% and the ink mass is almost completely lost. Accordingly, the DSC curve shows a sharp exothermic peak at about 725°C. The exothermic oxidation peak is surely due to the thermal degradation of the graphite into CO_2 and CO gases. Therefore, above 750°C, the ink is completely burned.

After several ink firing tests, it was found that a dwell time of 1h at 700°C was enough to completely remove the ink.

59

4.2.2 Rheological properties of the ink

Rheological properties if the ink have been analysed by rotational rheometer testing, the results are shown in the figure 4.12.

For pseudo-plastic or shear thinning fluids, the apparent viscosity decreases with increasing shear rates; the exponential decrease in apparent viscosity with increasing shear rates shown in the figure demonstrates that the PPG-graphite ink was highly shear thinning, as requested from a typical Robocasting ink.
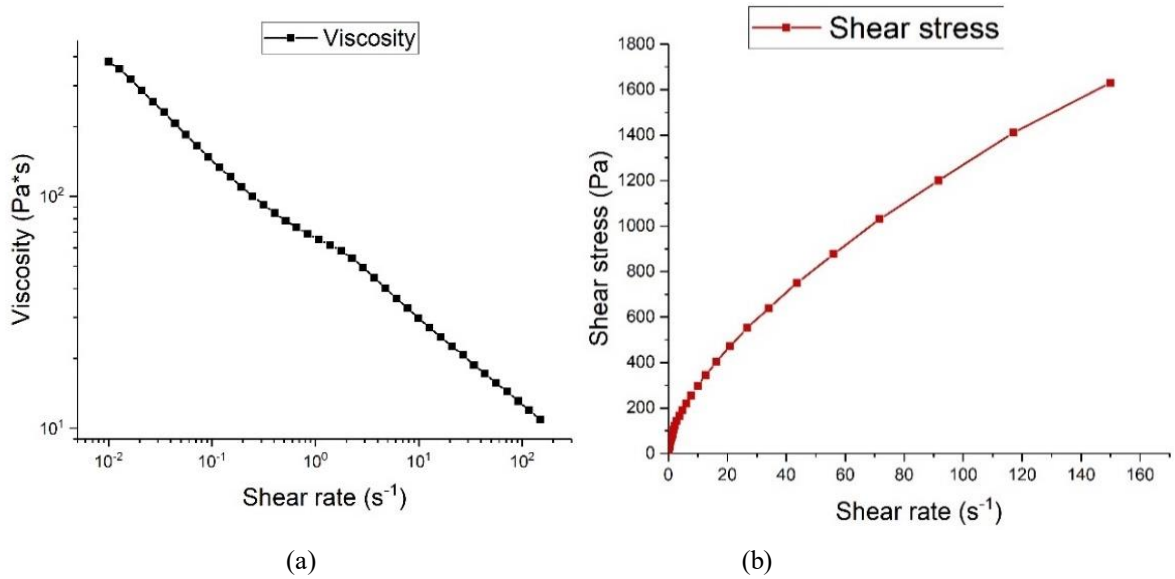

<div align="center">(a)   (b)</div>

Figure 4.12. *Log-log plot of evolution of apparent viscosity η_a (a) and Shear stress τ (b) as a function of shear rate $\dot{\gamma}$ for the ink.*

<div align="center">(a)   (b)</div>
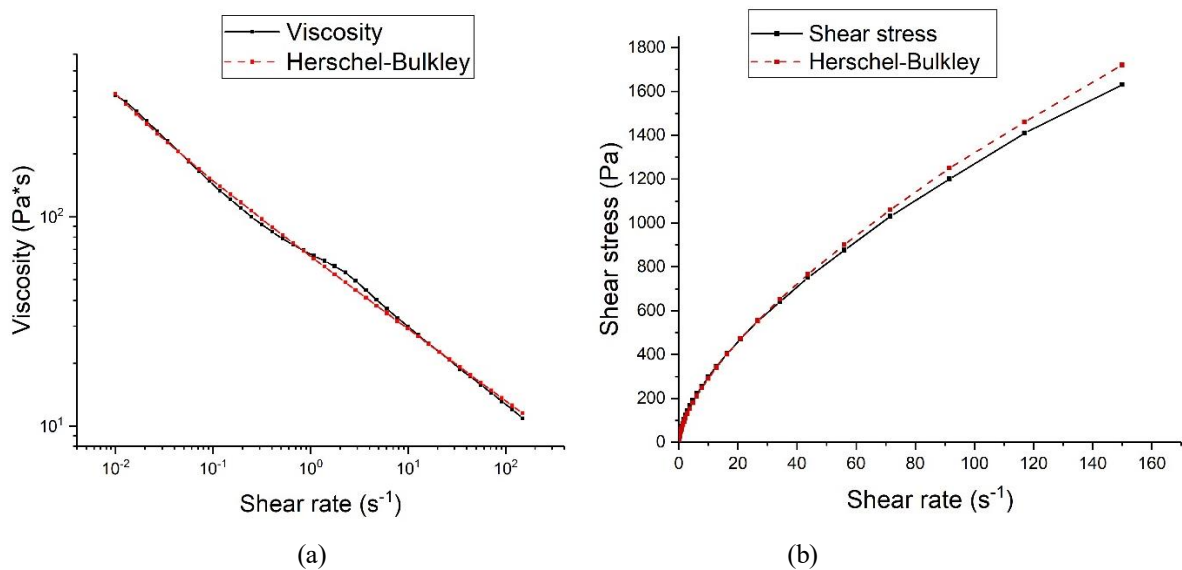
Figure 4.13. *Apparent viscosity (a) and shear stress (b) as a function of shear rate for the Herschel-Bulkley parameter interpolation.*

<div align="center">60</div>

The ink exhibited a positive and nearly zero yield stress ($\tau_y > 0$) and were shear thinning at stresses above the yield stress ($0 < n < 1$). The computed values for the Herschel-Bulkley model in Eq. 3.19 were $\tau_0 = 0,77831\ Pa$, consistency factor $k = 63,956$ and flow index of $n = 0,657$. From the figure 4.13 it can be noticed how the parameters of the Herschel-Bulkley model fit well with the experimental data, especially for viscosity. Ideally, an ink for direct ink writing should possess a higher yield stress in order to retain its shape one extruded and when multiple layers are stacked on top. However, in this case a lower (or absent) yield stress is acceptable and favourable: this way, the extruded ink can partially flow into the drilled channel filling it completely without leaving voids at the interface.

4.3   Process optimizations and results

The first results of the process showed evident defects in the part. Macroporosity, surface defects and an inadequate deposition of the slurry are visible in the figure 4.14a. Delamination was also observed especially between the layers below and above the channel but it was also present in other areas of the sample (Figure 4.15). The long time interval between the deposition of those layers was found to be the cause of this delamination: in fact, it was accentuated near the channels but anyway present throughout the entire interface between the layers.
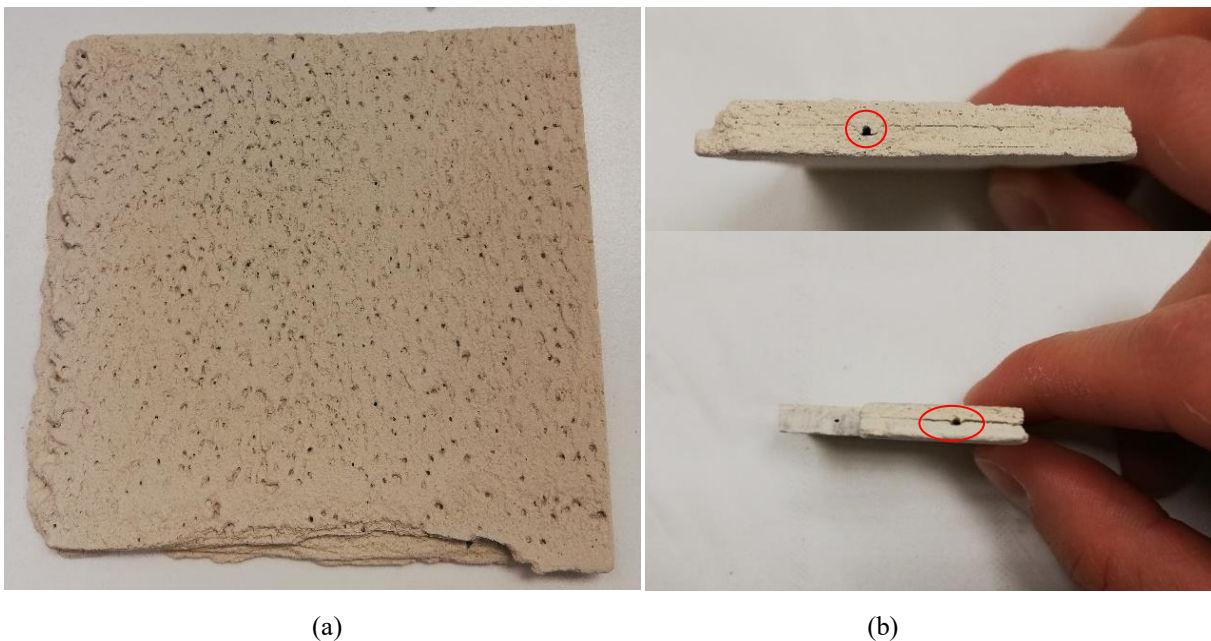

(a)   (b)

Figure 4.14. *Surface of green porcelain part by LSD process, it is visible a large amount of macro-porosity and surface defects (a), View of a portion of the channel after sintering, delamination at the channels is evident (b).*

The reason of such long interval resides in an approximate alignment of the worktop and of the robot in the hybrid deposition prototype. This caused a variation of the relative distance between

the tools (drilling and extruding tips) and the platform along the working platform; therefore, the distance needed to be adjusted manually before drilling and again before extrusion, in order to avoid differences in the channel depth and inhomogeneous ink deposition.

A further limitation of the equipment was the necessity to program different paths for drilling and extrusion phase, because of the different size and positioning of the tools. This also increased the process time.

Figure 4.15. Lateral view of the green LSD part, delamination is visible over the channel.

Another problem encountered was that the drill was not efficiently locked on the support, resulting in vibrations causing displacement of the dremel tip.
Figure 4.16 shows a computed tomography of the section of a sintered sample; it proves that the process worked as the channel was built and preserved inside the ceramic part; however, the drill tip displacement caused dimensional alterations along it.

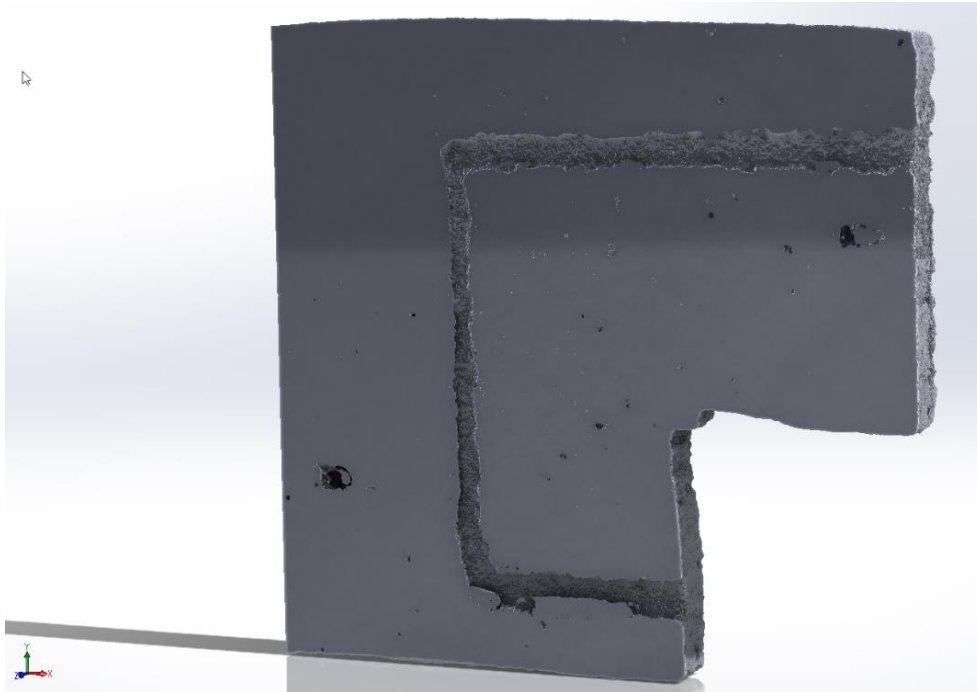To overcome these issues and improve the quality of the sample, several improvements have been made.

Figure 4.16. *Micro computed tomography (µCT) image of the cross-section of one of the first sintered parts obtained through the process developed in this project. The channel shows not regular shape.*

4.3.1 Equipment optimization

One of the main issues was height variation of the tool tip from the platform during robot movement, a map of this variation is reported in the figure 4.17. The plot doesn't cover the entire area of the platform because the robot, in the way it is placed, cannot reach all the portions of the platform.
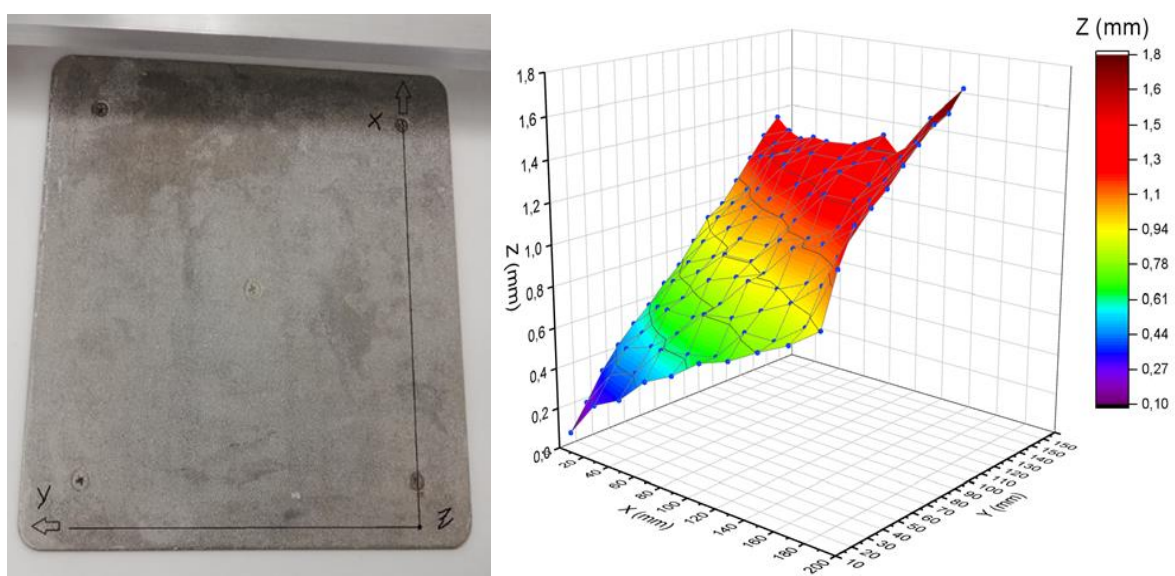

Figure 4.17. *Map of the change in position of the tip with the movement along the platform (Orientation of the robot A= 104,91 B= -87,46 C= 76,66).*

In order to minimize this variation and thus, minimize process times and the formation of delamination between the interface of the layers of first and second deposition process, the robot arm was rebalanced with spacers. Figure 4.18 maps the working area comparing the relative distance between the platform and the tool tip, before and after the adjustment; in the latter case the variation decreased to about 0,2 mm and was considered acceptable.

By testing deposition at increasing time intervals (from 20 to 120 minutes) between the first and second depositions step, it was observed that above half an hour of time interval delamination was visible. By reducing the interval between the two processes to less than 30 minutes, delamination was avoided or at least significantly minimized.

To minimize vibrations and the displacements of the tip of the drill during the work, an improved ABS support for the drill (see Figure 3.12) has been designed and 3D printed by means of a Renkforce RF2000 printer (Renkforce, Germany).
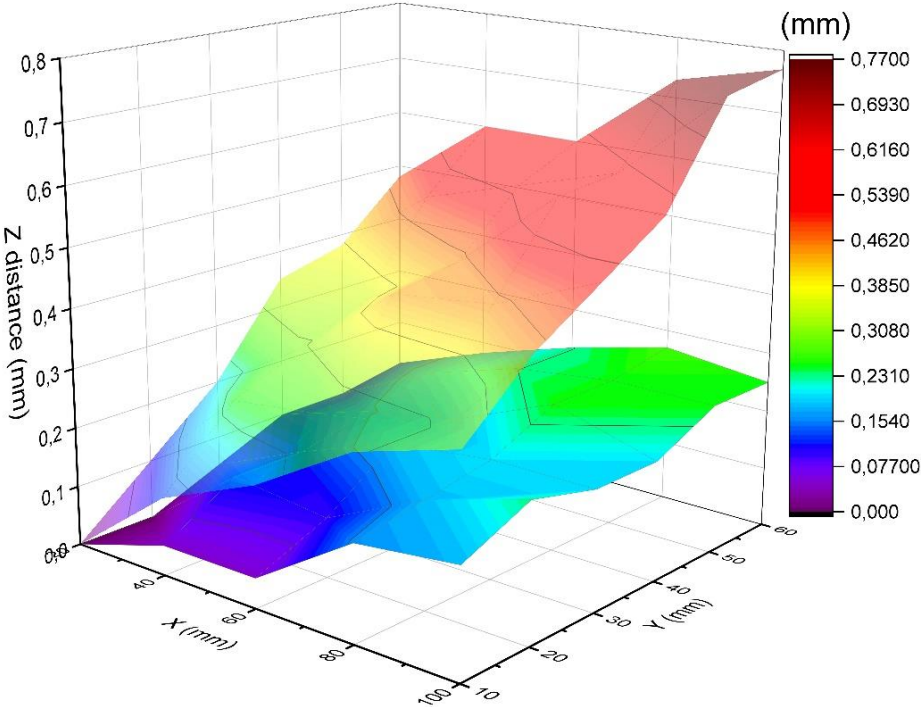

Figure 4.18. *Mapping area of interest before (upper) and after (lower) adjustments of the robot placement on the workstation.*

As regard deposition defects, it has been noted how important it was to stir the porcelain slurry with a mixer before starting deposition of the layers to avoid the presence of agglomerates, which could cause defects during the deposition. In addition, the viscosity of the slurry cannot be too high, as the layers were deposited by gravity

A further fundamental step, due to the machine setup, was to follow carefully the deposition and clean the doctor blade edges after each deposited layer, to avoid dried pieces of slurry which would cause scratches and damage the quality of the next layer. In addition, it was noted the importance of tapping the slurry inside the reservoir immediately before the deposition of each layer to avoid the presence of bubbles and to mix further the suspension.

Following these steps, better results were obtained in terms of deposition (Figure 4.19) and quality of the final ceramic parts.
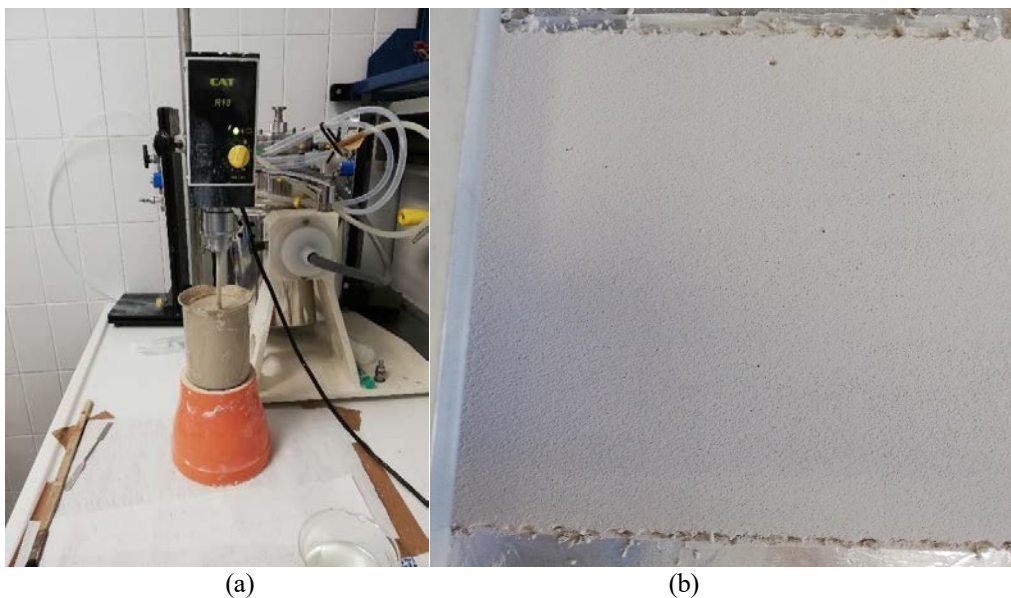

<div align="center">(a)   (b)</div>

Figure 4.19. *Mixing process of the slurry before filling the reservoir (a), surface green part made by LSD of porcelain with good surface quality and without significative macroporosity (b).*

4.3.2 Channel optimization and volumetric flow rate measurement

In order to optimize the size of the extruded ink filament with the theoretical one of the drilled channel, printing tests on porcelain substrate were conducted at different speeds of the extruder motor rotation (flow rate) and the extruded filament dimensions were estimated by image analysis. Figure 4.20 was used to estimate the width of the extruded filament using an image analysis software (ImageJ, USA). The amount of ink deposited (and consequently the line thickness) depends on the speeds of the robot arm (feed rate) and the extruder motor (flow rate). For convenience, the feed rate has been set at 10 mm/s and the flow has been adjusted at that speed.

For each strand, corresponding to a different rpm value of the extruder motor, the width was measured 10 times and the average value was chosen as the size of the extruded material filament. The following graph displays the estimated values: the increase in the width of the ink with the motor rotational speed is rather linear.
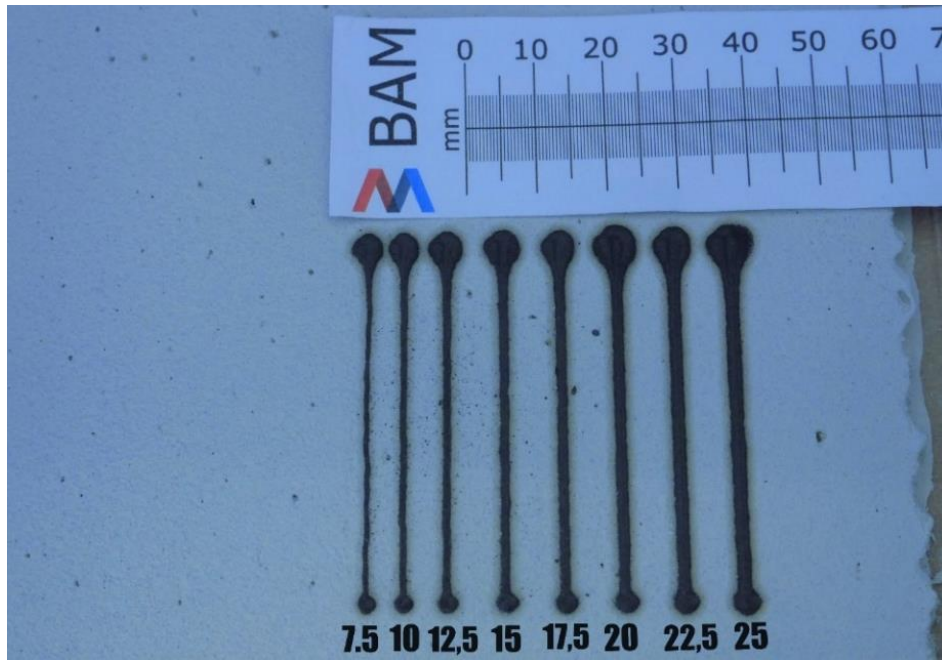
Figure 4.20. *Image of the ink deposition test at different rpm of the motor extruder used to analyze the size of the extruded filaments.*
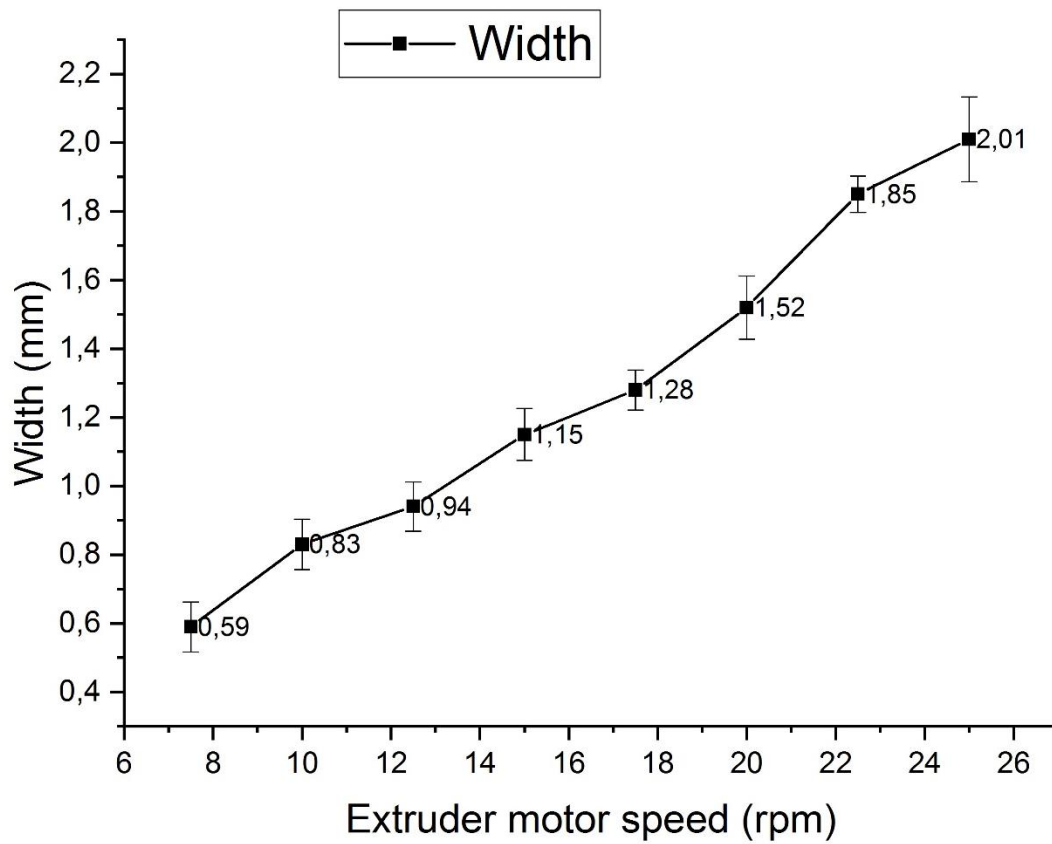

Figure 4.21. *Width of the extruded ink filament as a function of the extruder motor speed.*

Table 4.7. *Dimension of the ink filament for different motor speeds compared to those of the dug channel. The alternatives that best match the size of the channel are highlighted*

	Depth (mm)	Width (mm)	Volume per unit lenght (mm^3)
Channel	0,9	0,9	0,81
Ink (7,5 rpm)	0,75	0,59	0,44
Ink (10 rpm)	0,75	0,83	0,62
Ink (12,5 rpm)	0,75	0,94	0,71
Ink (15 rpm)	0,75	1,15	0,86
Ink (17,5 rpm)	0,75	1,28	0,96
Ink (20 rpm)	0,75	1,52	1,14
Ink (22,5 rpm)	0,75	1,85	1,39
Ink (25 rpm)	0,75	2,01	1,51

Establishing a channel depth of about 0.9 mm and a diameter of about 0.9 (diameter of the drill bit), the speeds that allow to have enough extruded material to best fill the channel are 12.5 and 15 rpm of the extruder, as outlined in the table 4.6.

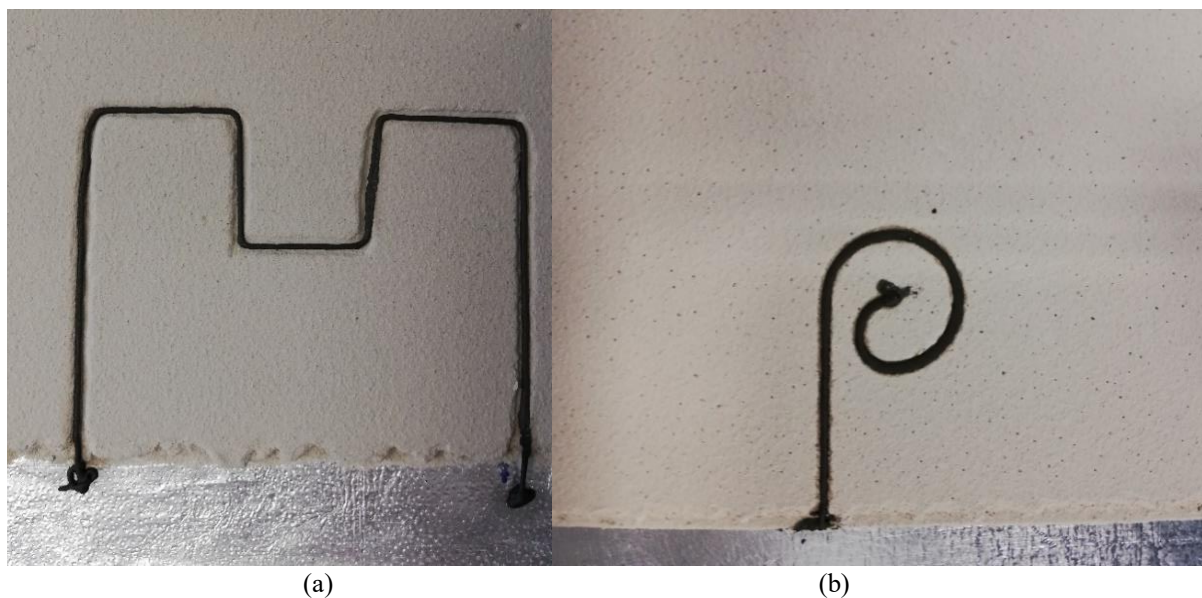(a)   (b)

Figure 4.22. Comparison between ink printing at 10 (a) and 15 (b) rpm of the extruder motor. The second picture visually shows that the ink completely fills the channel previously digged.

As shown in figure 4.22, it was important that the ink fills the bottom of the dug channel perfectly, in order to minimize the possibility of gaps and air bubbles during slurry deposition, which would result in cracks and defects in the channel at the end of the process.

As far as the drilling phase is concerned, as shown in the following figure, the depth and speed of the robot influenced the quality of the channel being forming. For depths of more than one mm, the weakness of the green porcelain did not allow to dig a regular channel, while, for the robot speed was visually noticed a better result for values of 10 or 12 mm/s compared to the lower speed, as shown in figure 4.23.
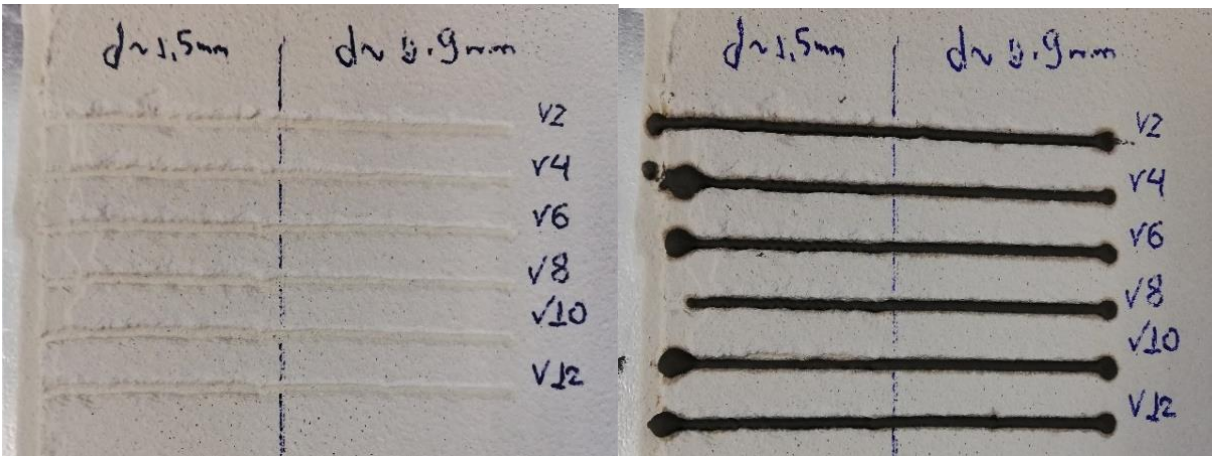

Figure 4.23. *Influence of the robot's motion speed and the drilling depth on the final visual quality of the channel to be built.*

The shear rate and stress values reached during the ink extrusion process can be calculated using the formulas reported chapter 3, but it is necessary to know the volumetric flow rate of the extrusion process. To measure the volumetric flow rate, a test for different working speeds of the extruder was carried out, as the flow rate obviously changed according to the working parameters of the motor.

As already mentioned, the tests consisted of extruding the graphite-ink into a vessel at different rpm of the motor for a time of 60 seconds and then measuring the mass of the extruded material. To estimate the volume of extruded material over time, it was necessary to measure the density of the ink, which depends on its components: graphite and PPG. The manufacturers of the materials involved did not provide precise density values, so it was preferred to measure it, weighing the mass of a certain volume of ink and thus obtaining its density (table 4.8).

Table 4.8. *Density measurement of the PPG-Graphite ink.*

PPG-Graphite ink	Volume (ml)	Mass (g)	Density (g/cm³)
	6	7,06	1,18

The mass of material extruded at each rpm was measured and, knowing the density, the corresponding volume was calculated and reported in Table 4.9; the volumetric flow rate (Q) and the shear rate values are reported in the table 4.10. The apparent ($\dot{\gamma}_a$) and true shear rate ($\dot{\gamma}_w$) at the nozzle wall were calculated according to Equations 3.16 and 3.17 respectively; in the latter case, the fluid flow index obtained from the interpolation was used ($n = 0,657$).

Table 4.9. *Mass and volume of extruded ink at different rpm of the motor in a minute time.*

Motor speed (rpm)	Mass extruded (g)	Extruded Volume (cm³)
7,5	0,27	0,23
10	0,37	0,31
12,5	0,44	0,37
15	0,53	0,45
17,5	0,63	0,54
20	0,71	0,60
22,5	0,82	0,70
25	0,92	0,78

Table 4.10 shows how a higher rpm value of the extruder corresponds to an increasing volumetric flow rate and a proportional increase of the shear rate. The true shear rate is higher as the ink flow index is n<1.

From the values of true shear rate reported above it was possible to obtain the corresponding values of viscosity and shear stress through the graphs obtained from the rheometric tests previously reported in Figure 4.12. Table 4.11 gives the values of the shear stress and of the viscosity of the ink corresponding to the working speed of the tool tested during the process.

For screw rotation speeds of 12.5 and 15 rpm inside the extruder, parameters that best match the previous drilling phase, the viscosity range of the ink during the extrusion process was very low as a result of the shear thinning behaviour of the fluid.

Table 4.10. *Volumetric flow rate, apparent and true shear rate of the ink at different working regime of the extruder.*

Motor speed (*rpm*)	Volumetric flow rate (*mm³/s*)	Apparent shear rate (*s⁻¹*)	Real shear rate (*s⁻¹*)
7,5	3,82	66,15	74,78
10	5,24	90,65	102,47
12,5	6,23	107,80	121,86
15	7,51	129,85	146,79
17,5	8,92	154,35	174,48
20	10,06	173,94	196,64
22,5	11,61	200,89	227,10
25	13,03	225,39	254,80

Table 4.11. *Rheological properties values of the ink during the extrusion process.*

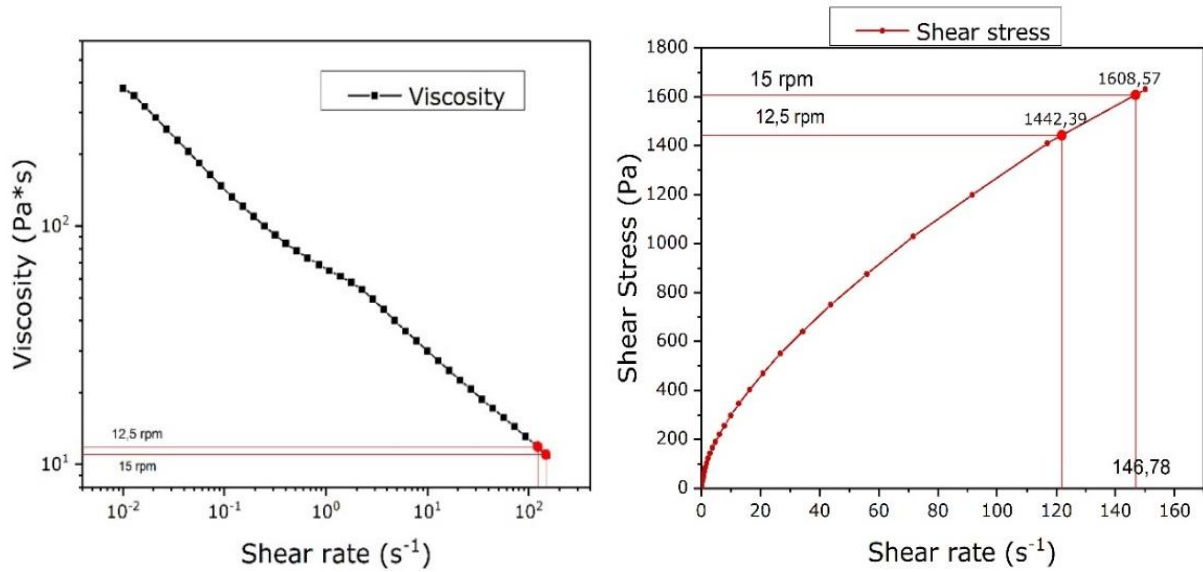| Motor speed (*rpm*)	Shear stress τ (*Pa*)	Apparent Viscosity η ($\textbf{\textit{Pa}} \cdot \textbf{\textit{s}}$)
7,5	1057,01	14,19
10	1289,89	12,63
12,5	1442,40	11,84
15	1608,57	11,01

Figure 4.24. *Viscosity and Shear stress values after interpolation of the shear rate parameters used during the working process.*

4.3.3 Microchannel parts investigation and results

In this paragraph are reported the results of microscope observations and x-ray micro-computed tomography to investigate the structure of produced ceramic parts with embedded microchannels.

As mentioned in chapter 2, the constrained shrinkage in the layer plane leads to biaxial stresses that can cause cracking in the material. The plasticity of clay materials ensures easy accommodation of these stresses during drying and porcelain slabs are particularly suitable for the LSD process.

In the figure 4.25 a rather layered structure with a good interface between layers, due to the slip casting process during the deposition, is visible in the cross section of the LSD green part. Since the ceramic slurry is extruded through a doctor blade, it can be noted that some larger grains were preferentially oriented along the deposition direction. The red arrow indicates the stacking direction of the layers.
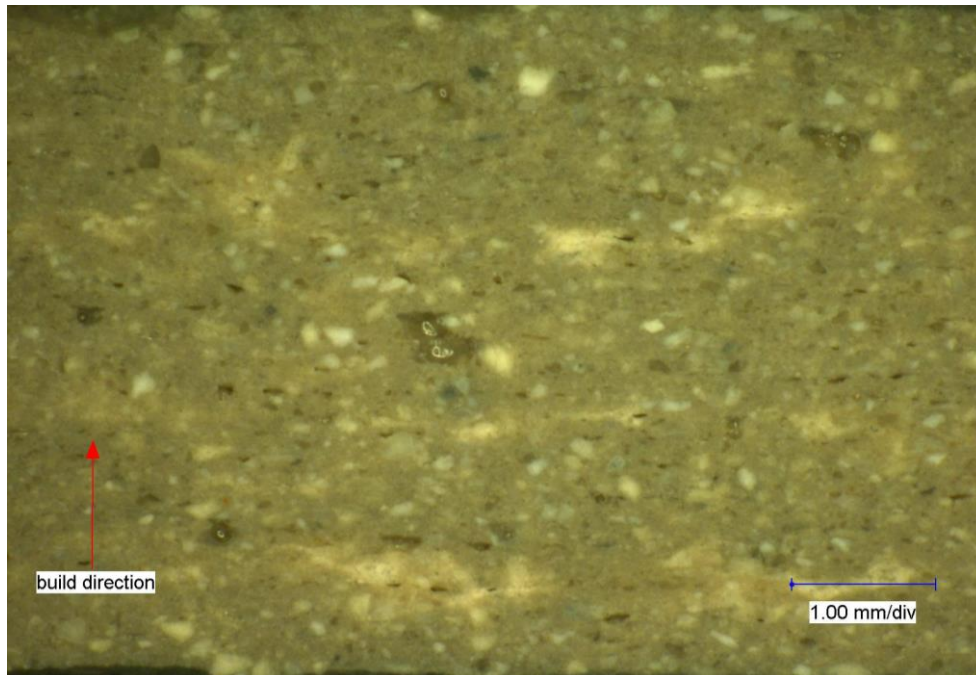
Figure 4.25. *Digital microscope image of the polished cross-section of LSD green sample. The arrow indicates the direction of stacking of the layers (Z direction).*

It was noticed that cracks in the proximity of the channel tended to develop after the firing of the samples and were considerably accentuated after the polishing and preparation of the samples for microscopic observation.

There are two main possible reasons for the formation of this defects: the first one could reside in the process times required between the slurry deposition below and above the channel: when the deposited layers dry too much, hindered shrinkage can develop stresses that cause delamination between the layers. This reason is less likely, since with the time optimization achieved delamination at the interface between layers was no longer visually present.

The second, more plausible, reason can be related to the characteristics of the ink, which may not be able to completely retain its cylindrical shape when covered with the next layer of slurry; it can be squeezed at the interface generating sharp edges upon firing. They can act as stress concentrators triggering crack propagation in a brittle material such as porcelain.

Figure 4.27 displays microscope images of channel embedded in a sample before and after the sintering and polishing treatments. It is possible to observe the growth of the crack after the heat treatment from the notches probably already present in the green structure.
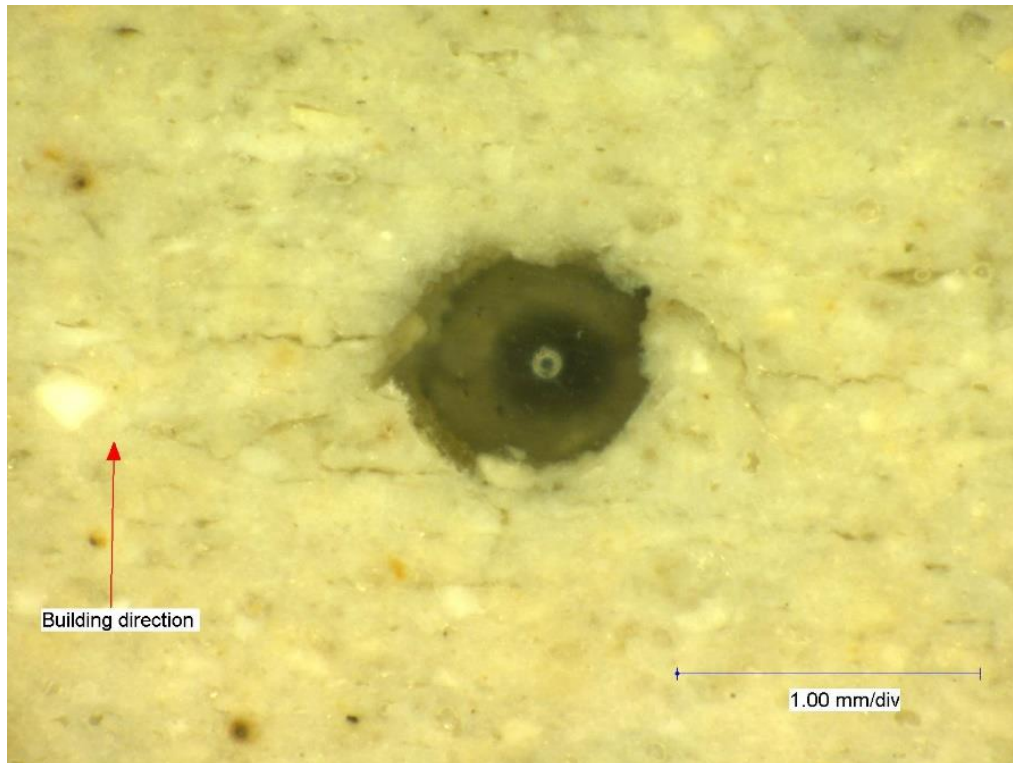
Figure 4.26. *Digital microscope image of the polished cross section of microchannel sample sintered at 1300°C/1h. The arrow indicates the direction of stacking of the layers (Z direction).*
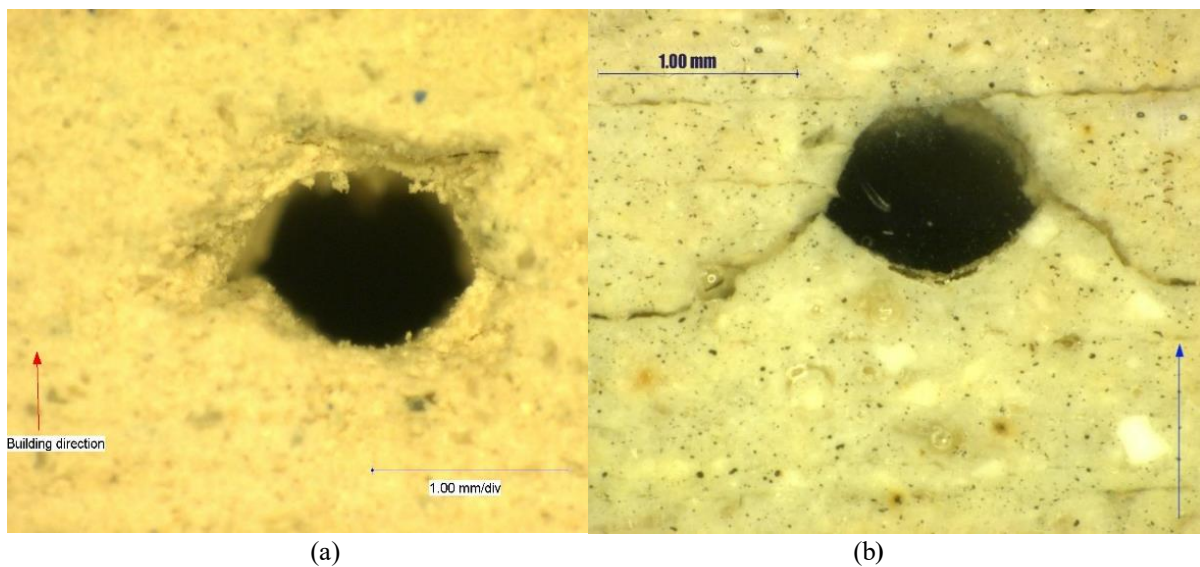

(a)   (b)

Figure 4.27. *Comparison between the digital microscope image of the cross-section of LSD green sample after firing at 700°C/1h, heat rate of 2°C/min, to eliminate the graphite inside the sample (a) and microscope image of the polished cross-section of the same sample after sintering at 1300°C/1h.*

Although the results of the channel in qualitative terms have not been optimal, the hybridization of AM technologies developed in this project has allowed to produce in a simplified way continuous channels with customizable paths inside ceramic slabs. Patterns can also be developed along the three dimensions: a simple example is shown in the Figure 4.28: the channel enters from the side of the tile and develops inside it until it exits from the top face. The image is obtained through VGSTUDIO software from μCT analysis elaboration.
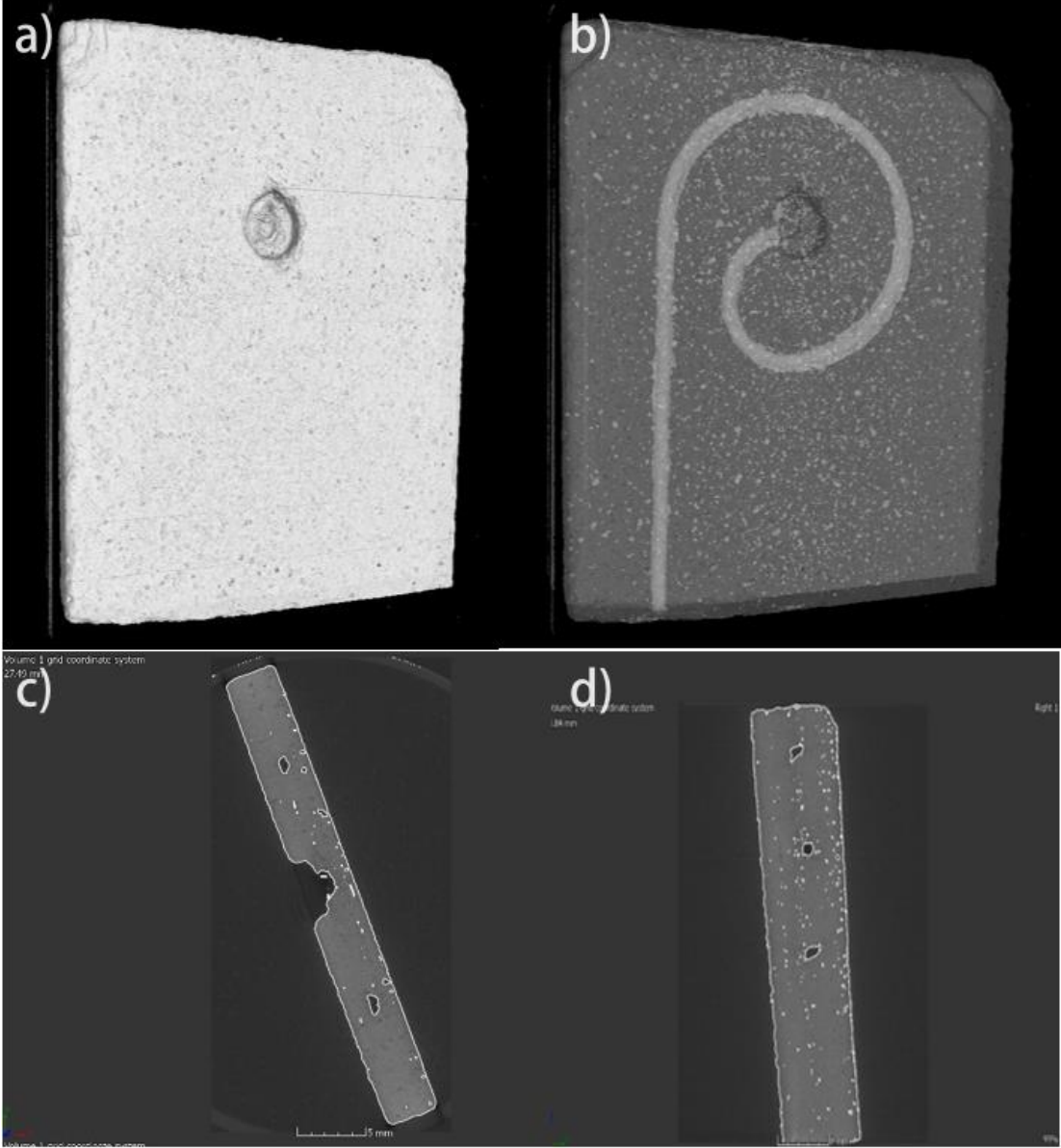

Figure 4.28. *Images by VGSTUDIO software of a ceramic sample with a built-in channel. Ceramic sample image where the exit hole of the channel is visible (a), upper cross-section image of the sample, where the path of the channel built inside is visible (b) and central (c) and cross sections (d) of the sample.*

Even if reduced, small porosities and defects were still visible in the ceramic slabs produced. Improvements to the process could be made in future works to significantly eliminate the presence of these defects. Designing a doctor blade more suitable for the process, connected to a pumping system that allows better packing and spreading of the slurry would significantly help to improve the quality of the deposition allowing also the use of advanced ceramic slurries.

Nevertheless, the hybrid technology thought for the aim of creating continuous millimetric openings in ceramic slabs has worked, the following image of some demonstration tests is also reported in support (Figure 4.29).

Figure 4.29. *Demonstration tests of the fluid flow inside the built channels.*

This process can certainly have further applications, such as the production of electrical circuits, by means of conductive inks, printed into ceramics generally insulating. In this case, the graphite-based ink prepared during this work was electrically conductive. By connecting a battery to the circuit formed by the ink path integrated inside the porcelain slab and a by a diode (figure 4.30), it was possible to observe the electric current flow and prove that the production of electric circuits within ceramics is an interesting future application of this technique.
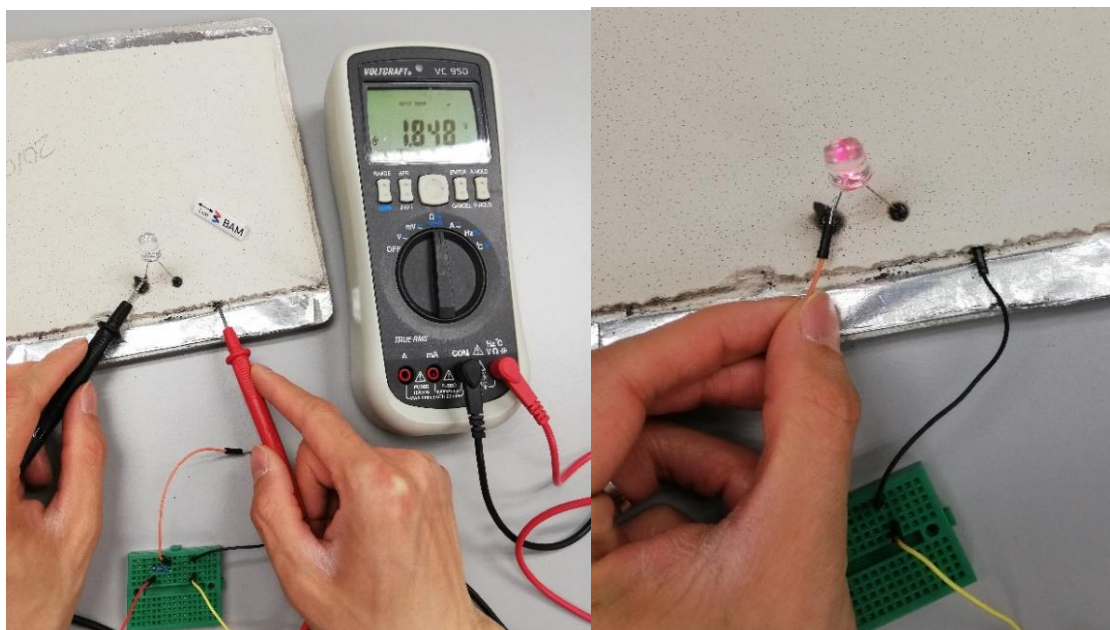
Figure 4.30. *Tests that prove the transfer of electrical current inside the LSD green porcelain slab through the circuit made up of the graphite ink previously deposited.*

Conclusions

This thesis work comprised the development of a novel technique based on the hybridization of AM technologies applied to ceramics, namely Layer-wise slurry deposition and Robocasting, to produce porcelain ceramic parts with embedded microchannel. This technology has been proved to be an alternative approach, in terms of simplicity and cost-effectiveness, to the traditional production techniques used at industrial level.

The LSD process has proved suitable for the deposition of porcelain slurry and production of ceramic slabs while a robot arm was used to dig the channels and print the ink inside them, in order to produce, after the firing process, channels integrated into the part. The PPG-graphite ink used has demonstrated rheological properties suitable for the robocasting process, which allowed it to have very low viscosity under stress during the extrusion process and an adequate shape retention capacity after the printing.

Optimization in the processes of slurry preparation, drilling phase and ink printing parameters were necessary to improve the results. After porosity and density measurements, the samples treated at 1300°C/1h were found to have the best characteristics and a microstructure composed mainly of quartz grains and mullite phase.

The results showed how this technology allowed to obtain microchannels with customizable paths, the high design freedom is one of the major advantages of AM processes. Being a prototype, there were however some process limitations. The main one was the presence of cracks and micro-fractures around the built channels, while a quality of the parts comparable to the one achievable by traditional industrial processes has not been achieved. Moreover, the simplicity of the machine didn't allow the use of advanced ceramic materials.

Future developments of this process would include the design and manufacture of a better doctor blade and associated pumping system, which would allow for higher quality depositions and finished parts, as well as the use of advanced ceramic slurries. Improvement of the machine could also comprise the automation of the same, in order to speed up the entire manufacturing process of the objects and reduce the failures due to the programming of the individual steps of deposition, drilling and printing. Further applications could include the manufacture of multi-material components but also the construction of electrical circuits made of conductive ink inside ceramic plates. In this case, electric conductive inks with a higher melting point than the sintering temperature of the ceramic material may be used.

Acknowledgements

I want to thank my parents Luigi and Angela before anyone else, for their constant support and for their sacrifices that allowed me to reach this goal. You are my role model.

A special thanks goes also to my brother Pierluigi, my grandparents and all aunts, uncles and cousins of my great family.

I would like to thank now the people I met during my internship at BAM, first of all Dr. Andrea Zocca for his supervision and help during the period and Prof. Jens Gunster for giving me the opportunity to work in a nice company and with a great team. Special thanks go to Raphael for his constant help and availability, as well as to Pedro and the other guys of the team.

I would also like to express my gratitude to Dr. Giorgia Franchin for her help in writing the thesis at the University of Padua and to Prof. Paolo Colombo for directing me towards this experience.

Last but not least, I thank all my friends, those of all time, for having always supported me and for all the joyful moments we spent together, the guys from the university, all the others known in Padova and the friends I met in Berlin for making this journey great.

Bibliography

1. K. F. Jensen / Chemical Engineering Science 56 (2001) 293}303
2. Lewinsohn CA, Wilson MA, Fellows JR, Anderson HS. Fabrication and joining of ceramic compact heat exchangers for process integration. Int J Appl Ceram Technol. 012;9(4):700–11.
3. Murphy DM, Manerbino A, Parker M, Blasi J, Kee RJ, Sullivan NP. Methane steam reformingn a novel ceramic microchannel reactor. Int J Hydrogen Energy. 013;38(21):8741 50.
4. Lewinsohn, Charles. (2015). High-efficiency, ceramic microchannel heat exchangers. American ceramic society Bulletin. 95. 26-31.
5. S. Annas, ''Advances in Low Temperature Co-Fired Ceramic (LTCC) for Ever Increasing Microelectronic Applications,'' 2003 IEEE Electronic Components and Technology Conference, New Orleans, LA, 1691–1693, 2003.
6. R. Kulka, M. Mittweger, P. Uhlig, and C. Gu¨nther, ''LTCC-Multilayer Ceramic for Wireless and Sensor Applications,'' IMST GmbH, http://www.ltcc.de, 2001.
7. S. Aviles and P. E. Vallejos, ''Medical Device Manufacturing and Technology—Processing of Materials for Biomedical Applications,'' Report, Electrical Engineering. University of Pennsylvania.
8. Birol, Hansu, Low temperature co-fired ceramic (LTCC) technology: general processing aspects and fabrication of 3-D structures for micro-fluidic devices
9. Yoshiniko I. ultilayered low temperature cofired ceramics technology. US: Springer; 2005.
10. Gongora-Rubio MR, Espinoza-Vallejos P, Sola-Laguna L, Santiago-Aviles JJ. Overview of low temperature co-fired ceramics tape technology for meso-system technology (MsST). Sens Actuat A: Phys 2001;89: 222–41.
11. Shafique MF, Laister A, Clark M, Miles RE, Robertson ID. Fabrication of embedded microfluidic channels in low temperature co‐fired ceramic technology using laser machining and progressive lamination. J Eur Ceram Soc. 2011;31(13):2199–204.
12. ASTM Standard F2792, Standard Terminology for Additive Manufacturing Technologies. ASTM International, West Conshohocken, Pennsylvania, 2012.
13. Gibson, D. W. Rosen, B. Stucker, *Additive Manufacturing Technologies*. Springer, New York, NY, 2015.
14. ISO/ASTM, 17296 Standard on Additive Manufacturing (AM) Technologies.
15. Deckers, J., Vleugels, J., Kruth, J.-P.: Additive manufacturing of ceramics: A review, J. Ceram. Sci. Tech., 5, 245 – 260, (2014).
16. Zocca, A. et al. Additive manufacturing of ceramics: issues, potentialities, and opportunities. Journal of the american ceramic society, v. 98, n. 7, p. 1983- 2001, jul. 2015.
17. Sachs, E.M., Haggerty, J.S., Cima, M.J., Williams, P.A.: United States patent 5.204.055: Three-dimensional printing techniques, (1993).
18. Kumar, S. JOM (2003) 55: 43. https://doi.org/10.1007/s11837-003-0175-y
19. Mühler, T. et al. Slurry-based powder beds for the selective laser sintering of silicate ceramics. Journal of ceramic science and technology, v. 6, n. 2, p. 113-118, abr. 2015.J.
20. Chiu, r. C.; garino, t. J.; cima, m. J.. Drying of granular ceramic films: i, effect of processing variables on cracking behaviour. Journal of the American ceramic society, v. 76, n. 9, p. 2257–2264, set. 1993.
21. Tarì, F. et al. Influence of solid loading on dryingshrinkage behaviour of slip cast bodies. Journal of the European ceramic society, v. 18, n. 5, p. 487–493, may. 1998.
22. https://www.euroceram.org/en/technologies/binder-jetting/slurry-based.html (last access 24.06.2019)
23. Lima, P., Journal of the European Ceramic Society (2018), https://doi.org/10.1016/j.jeurceramsoc.2018.03.014

24. Mühler, T. et al. Slurry-based additive manufacturing of ceramics. Internacional journal of applied ceramic technology, v. 12, n. 1, p. 18–25, jan. 2015.
25. Mühler, T. et al. Slurry-based powder beds for the selective laser sintering of silicate ceramics. Journal of ceramic science and technology, v. 6, n. 2, p. 113-118, abr. 2015.J.
26. https://www.additively.com/en/learn-about/fused-deposition-modeling (last access 24.06.2019)
27. Cesarano, P. D. Calvert, and Inventor: Sandia Corporation, Assignee,"Freeforming Objects with Low-Binder Slurry"; US Patent 6027326 A; February 22; US6027326 A, 2000.
28. Martinez-Vazquez FJ, Perera FH, Miranda P, Pajares A, Guiberteau F. Improving the compressive strength of bioceramic robocast scaffolds by polymer infiltration. Acta Biomater 2010, 6, 4361–8.
29. Miranda P, Saiz E, Gryn K, Tomsia AP. Sintering and robocasting of beta-tricalcium phosphate scaffolds for orthopaedic applications. Acta Biomater 2006, 2, 457–466.)
30. Francisco J. Martínez-Vázquez, Antonia Pajares, Pedro Miranda A simple graphite-based support material for robocasting of ceramic parts. Journal of European Ceramic Society, 2018.
31. Standard Definition of Terms Related to Ceramic Whitewares and Related Products," ASTM Designation C 242. *I996 Annual Book of ASTM Standards,* Vol. 15.02. American Society for Testing and Materials, Philadelphia, PA.
32. W.M. Carty, U. Senapati, Porcelain - raw materials, processing, phase evolution, and mechanical behavior, J. Am. Ceram. Soc. 81 (1) (1998) 3–20.
33. Malvern & Spectrics, 2015
34. ISO 18754: Fine ceramics (advanced ceramics, advanced technical ceramics) - Determination of density and apparent porosity. (2013).
35. M.J. Orts, A. Escardino, J.L. Amorós, F. Negre, Microstructural changes during the firing of stoneware floor tiles, Appl. Clay Sci. 8 (2) (1993) 193–205.